# Mixed analytic/energetic approach for a sliding orthotropic hollow cylinder. Application to coil sagging

Daniel Weisz-Patrault, Maxime Gantier, Alain Ehrlacher

# Mixed analytic/energetic approach for a sliding orthotropic hollow cylinder. Application to coil sagging

Daniel Weisz-Patrault[a], Maxime Gantier[b], Alain Ehrlacher[b]

[a]*LMS, École Polytechnique, CNRS, Université Paris-Saclay, 91128 Palaiseau, France*
[b]*Laboratoire Navier, CNRS, École Ponts ParisTech, 6 & 8 Ave Blaise Pascal, 77455 Marne La Vallée, France*

**Abstract**

This paper deals with the numerical simulation of coil sagging. This problem arises within the framework of the steel making industry where strips are wound on themselves for storage. Coil sagging is a major defect that can occur for recent grades undergoing phase transitions during the coiling process. The detailed mechanisms leading to coil sagging are still not well understood, making this phenomenon very difficult to prevent. The coil is a multilayer hollow cylinder where sliding takes place at each interface and significantly contributes to the overall deformation. However, a detailed numerical simulation addressing the contact problem, considering both pressure and sliding is difficult to perform under non-axisymmetric conditions. This paper presents a simplified approach considering an orthotropic hollow cylinder instead of a multilayer coil. The anisotropy is due to contact roughness that tends to decrease the radial stiffness. The hollow cylinder is subjected to gravity and an eigenstrain representing thermal expansion, phase transitions and transformation induced plasticity. Sliding at each interface is taken into account through a continuous plastic-like shear strain that is determined through an energetic principle. The proposed solution relies on analytical developments so that computation time is compatible with parametric studies. Results are addressed in order to give a better understanding of mechanisms and conditions under which coil sagging occur.

*Keywords:* Energetic approach, orthotropy, Residual stress, Eigenstrain, Coil sagging

## 1. Introduction

The current dynamic of steel manufacturing is to regularly develop new stronger grades enabling users to reduce strip thicknesses and thus reduce produced tonnages, which participates to the energy efficiency by minimizing for instance the total mass of vehicles etc. One of the major issues related to this evolution of steel production is the forming processes that lead to serious residual stress problems which in turn can result in major defects. This contribution focuses on the coiling process, which consists in winding a strip on itself for storage. Within this framework, non axi-symmetric deformations can result in coil sagging, as demonstrated in figure 1. Other defects are described in Edwards and Boulton (2001). Coil sagging is a major defect that can occur for recent grades undergoing phase transitions during the coiling process. The detailed mechanisms leading to coil sagging are still not well understood making this phenomenon very difficult to prevent. Besides gravity that seems to play a role, phase transitions are often associated to coil sagging because it occurs mostly for grades that undergo structural transformation during the coiling process. This paper is an attempt to develop a numerical tool in order to identify critical loading conditions leading to coil sagging and to explain main

deformation mechanisms involved. In particular, to what extent gravity or some imposed eigenstrain conditions representing thermal expansion, phase transitions and transformation induced plasticity may be responsible for the coil sagging phenomenon ?

Figure 1: Coil sagging

The coil can be described as an axi-symmetric multilayer hollow cylinder for which each layer is considered individually with contact conditions. For instance, Weisz-Patrault et al. (2016) proposed a non-linear elastic-plastic winding model, accounting for roughness of contacts and finite strain in order to consider large rotations. This model was based on previous contributions proposed by Weisz-Patrault and Ehrlacher (2017) and Weisz-Patrault et al. (2015). Then, Weisz-Patrault (2017a) developed a thermal solution for a coil under cooling conditions, by coupling heat conduction and multiphase transition problems accounting for thermal contact resistance at each interface. Recently, Weisz-Patrault (2018) established a numerical strategy in order to compute residual stresses and inelastic strains generated during cooling, on the basis of the previously developed models. Each layer of the coil is subjected to an eigenstrain increment denoted by $\boldsymbol{\varepsilon}^{*,(j)}$ (where $(j)$ refers to the layer index) composed of several contributions detailed by Weisz-Patrault (2017b), namely:

(1) thermo-metallurgical hydrostatic strain due to thermal expansion and density mismatch between different phases
(2) transformation induced plastic strain
(3) classical plastic strain due to temperature variations

It should be noted that both the transformation induced plastic strain rate and the classical plastic strain rate due to temperature variations are proportional to the overall deviatoric stress. Thus, the imposed eigenstrain depends significantly on the stress state of the previous time step, leading to a non-linear evolution. This imposed eigenstrain is the main load during cooling.

Together, these papers form a comprehensive numerical tool that enables us to quantify -under axi-symmetric conditions- inelastic strains[1] taking place when the coil is wound and cooled down. However, coil sagging implies a loss of the axial symmetry, as shown in figure 1, that is often attributed to gravity. This paper is an attempt to develop a numerical tool to deal with non-axi-symmetric conditions and sliding in order to address coil sagging issues.

[1]The whole mechanical state is determined, stress and strain, displacement, contact pressures etc...

However, considering all layers individually and computing both contact pressure and sliding at each interface is difficult under non axi-symmetric conditions. A simplified approach is proposed in this paper. The coil is modeled as a homogenized orthotropic hollow cylinder under plane strain assumption. Layers are not considered individually but as a continuum. The orthotropy of the homogenized model is due to the fact that contact roughness tends to decrease the radial stiffness as observed for instance by Wadsley and Edwards (1977), Edwards and Boulton (2001), Hudzia et al. (1994) or Kedl (1992). Consider the 4-order stiffness tensor $\boldsymbol{C}$ such as $\boldsymbol{\sigma} = \boldsymbol{C} : \boldsymbol{\varepsilon}^e$ where $\boldsymbol{\sigma}$ is the Cauchy stress tensor and $\boldsymbol{\varepsilon}^e$ the elastic strain tensor. Considering the plane strain assumption, the orthotropic behavior is written using the Voigt notation:

$$\begin{bmatrix} \sigma_{rr} \\ \sigma_{\theta\theta} \\ \sigma_{r\theta} \end{bmatrix} = \begin{pmatrix} C_{11} & C_{12} & 0 \\ C_{12} & C_{22} & 0 \\ 0 & 0 & C_{66} \end{pmatrix} . \begin{bmatrix} \varepsilon^e_{rr} \\ \varepsilon^e_{\theta\theta} \\ 2\varepsilon^e_{r\theta} \end{bmatrix} \tag{1}$$

where:

$$C_{11} = \frac{\lambda + 2\mu}{\alpha^2} \;\Big|\; C_{22} = \lambda + 2\mu \;\Big|\; C_{12} = \lambda \;\Big|\; C_{66} = \mu \tag{2}$$

where $(\lambda, \mu)$ are the Lamé's coefficients and $\alpha \geq 1$ is introduced in order to decrease the radial stiffness. It should be mentioned that $\boldsymbol{C}$ needs to be positive definite so that the elastic bulk energy is positive. This condition implies that $\alpha$ lies in the range:

$$\alpha \in \left[1, \frac{\lambda + 2\mu}{\lambda}\right] \tag{3}$$

Since the coil is composed of a large number of layers (several hundreds), sliding is taken into account through a continuous plastic-like shear strain instead of discrete slips denoted by:

$$\boldsymbol{\varepsilon}^p = \frac{\gamma^p}{2} \left(\boldsymbol{e_r} \otimes \boldsymbol{e_\theta} + \boldsymbol{e_\theta} \otimes \boldsymbol{e_r}\right) \tag{4}$$

A clear limitation of the proposed homogenized approach is to allow for radial tension although the non-homogenized problem would result in contact loss instead (as in figure 1). In addition, this paper does not deal with post-bifurcation regime and mainly focuses on sliding between layers, even though in real coils, local buckling may occur and lead to contact loss due to compressive stresses in thin layers. Despite these modeling limitations, the main mechanism to predict coil sagging as a structural effect is identified to be sliding between layers, which is captured by $\gamma^p$ in the proposed approach. In this paper, non-linearity is limited to the determination of $\gamma^p$. Thus, the continuous model does not enable each layer to undergo plastic deformation due to strong curvature for instance. However, results suggest that sliding leads to coil sagging with fairly small equivalent stresses. Finite strains (geometrical non-linearity) have not been considered either for the sake of simplicity. This could introduce a bias on the exact final shape, but the infinitesimal strain assumption still enables to identify whether coil sagging occurs under certain conditions, which is the main purpose of the proposed approach.

Sliding is responsible for dissipation, thus a dissipation is associated to the continuous plastic-like shear strain that is determined through an energetic principle. The total energy to be minimized is composed of the elastic bulk energy $E\left[\gamma^p\right]$ minus the work of external forces $W\left[\gamma^p\right]$ plus the plastic-like dissipated energy $D\left[\gamma^p\right]$. A similar approach has been used for instance by Bluthé et al. (2017) within a different context. The dissipation can be interpreted as a cost to reach a lower energy state as detailed by Fedelich and Ehrlacher (1997) and Mielke

(2003). The minimization procedure is detailed in section 6. The proposed approach relies on an analytical solution of the orthotropic hollow cylinder, in order to obtain computation time compatible with parametric studies.

In addition, coil sagging is a structural effect due to non axi-symmetric loading conditions such as gravity or if the imposed eigenstrain is inhomogeneous along the circumferential direction because of cooling conditions that can be slightly off the axi-symmetric assumption. A simple question arises: is gravity sufficient to be responsible for such a dramatic loss of axi-symmetry and to what extent does the eigenstrain dependence on the circumferential direction contribute to the phenomenon ? A Fourier series expansion of the imposed eigenstrain in each layer is considered:

$$\boldsymbol{\varepsilon}^{*,(j)}(r,\theta) = \sum_{n=-N}^{N} \boldsymbol{\varepsilon}_n^{*,(j)}(r)\exp(in\theta) \tag{5}$$

Since the effect of the axi-symmetric term $\boldsymbol{\varepsilon}_0^{*,(j)}$ is already captured by the model developed by Weisz-Patrault (2018), the structural effect leading to coil sagging is given only by the non axi-symmetric terms $\boldsymbol{\varepsilon}_n^{*,(j)}$ $(n \neq 0)$ in the Fourier series expansion. The homogenized imposed eigenstrain $\boldsymbol{\varepsilon}^*$ is defined as follows:

$$\boldsymbol{\varepsilon}^{*}(r,\theta) = \sum_{\substack{n=-N \\ n\neq 0}}^{N} \boldsymbol{\varepsilon}_n^{*}(r)\exp(in\theta) \tag{6}$$

where $\boldsymbol{\varepsilon}_n^*$ is interpolated through cubic splines between following values:

$$\boldsymbol{\varepsilon}_n^*(r^{(j)}) = \frac{1}{r_{sup}^{(j)} - r_{inf}^{(j)}} \int_{r_{inf}^{(j)}}^{r_{sup}^{(j)}} \boldsymbol{\varepsilon}_n^{*,(j)}(r)\mathrm{d}r \tag{7}$$

where $r^{(j)} = (r_{sup}^{(j)} + r_{inf}^{(j)})/2$. This simple homogenization procedure is summarized in figure 2.

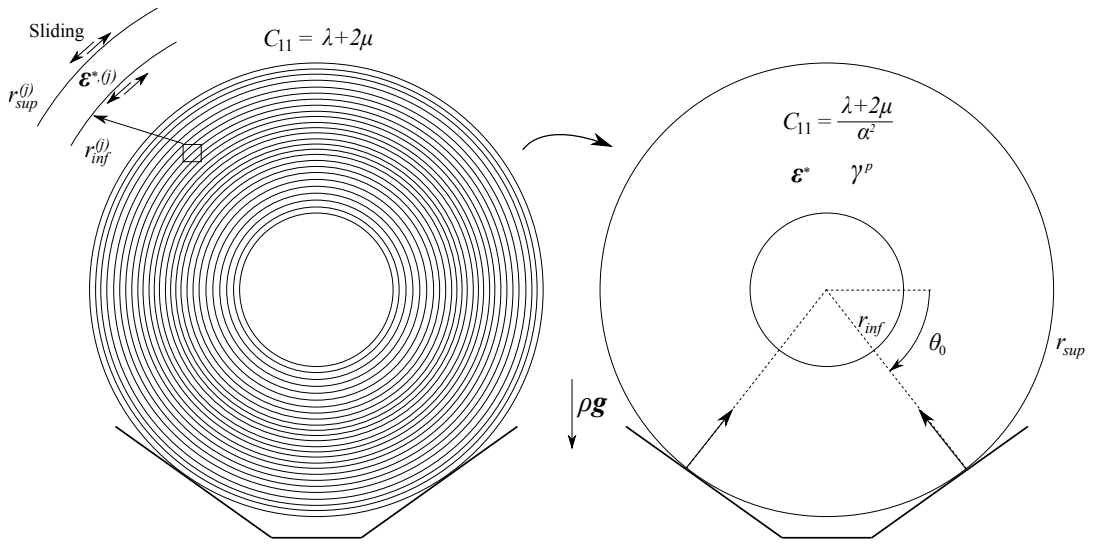


Figure 2: Homogenization

Thus, the proposed approach relies on the derivation of an analytical solution of an orthotropic hollow cylinder subjected to gravity and an imposed eigenstrain as well as a plastic-like shear strain that is determined in the end by an energetic principle. Many contributions focus on this kind of mechanical configuration. For instance, for isotropic hollow cylinders and plastic deformations (without energetic considerations), Bree (1989) developed a bi-axial analytical solution for a pressurized tube using the Tresca yield function and where stresses are averaged through the thickness. Eraslan and Akis (2006) gave an analytical solution for a functionally graded elastic-plastic pressurized tube and Chatzigeorgiou et al. (2009) published an homogenization of a multilayer elastic-plastic pressurized tube with discontinuous material properties. Pronina (2013) developed an analytical solution of an elastic-plastic pressurized tube considering mechanochemical corrosion. Furthermore, orthotropic hollow cylinders have also been studied. For instance, Pagano (1994) developed an analytical solution for an anisotropic hollow cylinder subjected to surface traction expressed in the form of a Fourier series expansion. Kalam and Tauchert (1978) proposed an analytical solution for an orthotropic hollow cylinder with a spherical eigenstrain (proportional to the identity) due to thermal expansion. The solution relies on the Airy potential, Fourier series expansions and power series along the radial direction. Kardomateas (1990) and Yee and Moon (2002) proposed analytical solutions to a similar problem considering respectively Hankel asymptotic expansions and Bessel functions. El-Naggar et al. (2002) proposed a Finite Difference method in order to solve a rotating orthotropic hollow cylinder subjected to thermal expansion. Ye and Soldatos (1994) proposed a analytical solution relying on Fourier series expansion for a three-dimensional multilayer hollow cylinder transversely loaded. Other kinds of eigenstrains have also been considered. For instance Hou and Leung (2004) developed a semi-analytical dynamic solution for magneto-electro-elastic orthotropic hollow cylinders. Magneto-thermoelastic problem for rotating orthotropic hollow cylinders has been proposed by Abd-Alla and Mahmoud (2010) and solved numerically through an implicit finite-difference scheme.

The present analytical solution is developed for general eigenstrain and relies on orthogonal series expansions using Bessel functions of the first and second kinds. However, it should be noted that isotropic plane problems can be usefully written within the framework of complex analysis as demonstrated by Muskhelishvili (1953). Incomplete extensions to anisotropic materials have been developed by Lekhnitskii et al. (1964) and involve two complex variables instead of one. A unified and complete complex theory for plane problems has been published by Ou and Chen (2007). Weisz-Patrault et al. (2014) also proposed an extension in 3D of the Kolosov-Muskhelishvili formulation using the four-dimensional hyper-complex algebra of quaternions. However to the best of our knowledge no 3D formulation has been published for anisotropic elasticity by using hyper-complex potentials.

## 2. Global equations and problem decomposition

This section deals with the global equation system and boundary conditions. The orthotropic hollow cylinder is subjected to an imposed eigenstrain (which is an input of the model) and a plastic-like shear strain defined by (4) and determined in the end by a minimization procedure detailed in section 6. Thus, the plastic-like shear strain $\gamma^p$ can be considered as an imposed parametric eigenstrain, until section 6 where an energetic principle is stated to

determine $\gamma^p$. The following equation system should be solved:

$$\begin{cases} \mathbf{div}\left[\boldsymbol{\sigma}\right] = \rho g \boldsymbol{e}_y & \text{Equilibrium} \\ \boldsymbol{\sigma} = \boldsymbol{C} : \boldsymbol{\varepsilon}^e & \text{Orthotropic behavior} \\ \boldsymbol{\varepsilon} = \dfrac{1}{2}\left(\boldsymbol{\nabla}\left[\boldsymbol{u}\right] + \boldsymbol{\nabla}\left[\boldsymbol{u}\right]^T\right) & \text{Compatibility} \\ \boldsymbol{\varepsilon}^e = \boldsymbol{\varepsilon} - \boldsymbol{\varepsilon}^* - \boldsymbol{\varepsilon}^p & \text{Elastic strain tensor} \end{cases} \tag{8}$$

where $\rho$ denotes the density, $g$ the acceleration of gravity, $\boldsymbol{\sigma}$ is the stress tensor, $\boldsymbol{\varepsilon}$ is the total strain tensor, $\boldsymbol{u}$ is the displacement vector, $\boldsymbol{\varepsilon}^e$ is the elastic strain tensor, $\boldsymbol{\varepsilon}^*$ is the imposed eigenstrain and $\boldsymbol{\varepsilon}^p$ the plastic like shear strain and $\boldsymbol{C}$ is the stiffness tensor.

Following boundary conditions are considered:

$$\begin{cases} \boldsymbol{\sigma}(r_{sup}, \theta).\boldsymbol{n} = \boldsymbol{T} = T_r^{sup}(\theta)\boldsymbol{e}_r \\ \boldsymbol{\sigma}(r_{inf}, \theta).\boldsymbol{n} = 0 \end{cases} \tag{9}$$

where $\boldsymbol{n}$ is the normal unit vector and:

$$T_r^{sup}(\theta) = -\frac{\pi\left(r_{sup}^2 - r_{inf}^2\right)\rho g}{2\sin(\theta_0) r_{sup}}\left(\delta_{\theta_0}(\theta) + \delta_{\pi-\theta_0}(\theta)\right) \tag{10}$$

where $\theta_0$ is the angle that defines contact points with the support and $\delta$ denotes the Dirac distribution. $T_r^{sup}$ is defined so that the resultant force due to gravity is balanced symmetrically on both supports as shown in figure 2. Detailed calculation is given in Appendix A.

It is convenient to write the equilibrium equation on displacements instead of stresses. The obtained equation is called the inhomogeneous Navier equation and reads for the assumed orthotropic behavior (2):

$$\begin{cases} (\lambda+2\mu)\left(\dfrac{1}{\alpha^2}\left(\dfrac{\partial^2 u_r}{\partial r^2} + \dfrac{1}{r}\dfrac{\partial u_r}{\partial r}\right) - \dfrac{u_r}{r^2}\right) + \mu\dfrac{1}{r^2}\dfrac{\partial^2 u_r}{\partial\theta^2} + (\lambda+\mu)\dfrac{1}{r}\dfrac{\partial^2 u_\theta}{\partial r\partial\theta} - (\lambda+3\mu)\dfrac{1}{r^2}\dfrac{\partial u_\theta}{\partial\theta} = \mu\left(f_r^* + f_r^p\right) + \rho g\sin(\theta) \\ \mu\left(\dfrac{\partial^2 u_\theta}{\partial r^2} + \dfrac{1}{r}\dfrac{\partial u_\theta}{\partial r} - \dfrac{u_\theta}{r^2}\right) + (\lambda+2\mu)\dfrac{1}{r^2}\dfrac{\partial^2 u_\theta}{\partial\theta^2} + (\lambda+\mu)\dfrac{1}{r}\dfrac{\partial^2 u_r}{\partial r\partial\theta} + (\lambda+3\mu)\dfrac{1}{r^2}\dfrac{\partial u_r}{\partial\theta} = \mu\left(f_\theta^p + f_\theta^*\right) + \rho g\cos(\theta) \end{cases} \tag{11}$$

where:

$$\begin{cases} f_r^*(r,\theta) = \dfrac{\lambda+2\mu}{\alpha^2\mu}\dfrac{\partial\varepsilon_{rr}^*}{\partial r} + \dfrac{\lambda}{\mu}\dfrac{\partial\varepsilon_{\theta\theta}^*}{\partial r} + 2\left(\dfrac{\varepsilon_{rr}^* - \varepsilon_{\theta\theta}^*}{r} + \dfrac{1}{r}\dfrac{\partial\varepsilon_{r\theta}^*}{\partial\theta}\right) + \dfrac{\lambda+2\mu}{\mu}\dfrac{(1-\alpha^2)}{\alpha^2}\dfrac{\varepsilon_{rr}^*}{r} \\ f_\theta^*(r,\theta) = \dfrac{\lambda}{\mu r}\dfrac{\partial\varepsilon_{rr}^*}{\partial\theta} + \dfrac{\lambda+2\mu}{\mu r}\dfrac{\partial\varepsilon_{\theta\theta}^*}{\partial\theta} + 2\left(\dfrac{\partial\varepsilon_{r\theta}^*}{\partial r} + \dfrac{2\varepsilon_{r\theta}^*}{r}\right) \end{cases} \tag{12}$$

and where:

$$\begin{cases} f_r^p(r,\theta) = \dfrac{1}{r}\dfrac{\partial\gamma^p}{\partial\theta} \\ f_\theta^p(r,\theta) = \dfrac{\partial\gamma^p}{\partial r} + \dfrac{2\gamma^p}{r} \end{cases} \tag{13}$$

Despite the fact a plastic-like shear strain $\gamma^p$ is considered, the inhomogeneous Navier equation (11) is linear. Indeed, usually plastic strains are dependent on the unknown displacement $\boldsymbol{u}$, however the derivation of the analytical solution is done with an arbitrary shear strain $\gamma^p$ that does not depend on $\boldsymbol{u}$. Thus, all non-linear aspects are handled through the final minimization

task that enables to determine $\gamma^p$, as detailed in section 6. Therefore, the solution of (11) with boundary conditions (9) can be split into several contributions denoted by:

$$\left\{\begin{array}{l} \boldsymbol{u} = \boldsymbol{u}^* + \boldsymbol{u}^p + \boldsymbol{u}^W + \widehat{\boldsymbol{u}} \\ \boldsymbol{\varepsilon} = \boldsymbol{\varepsilon}^* + \boldsymbol{\varepsilon}^p + \boldsymbol{\varepsilon}^W + \widehat{\boldsymbol{\varepsilon}} \\ \boldsymbol{\sigma} = \boldsymbol{\sigma}^* + \boldsymbol{\sigma}^p + \boldsymbol{\sigma}^W + \widehat{\boldsymbol{\sigma}} \end{array}\right. \tag{14}$$

Displacement vectors $\boldsymbol{u}^*$ and $\boldsymbol{u}^p$ are any particular solution (without specifying specific boundary conditions) of:

$$\left\{\begin{array}{l} (\lambda+2\mu)\left(\frac{1}{\alpha^2}\left(\frac{\partial^2 u_r^{(.)}}{\partial r^2}+\frac{1}{r}\frac{\partial u_r^{(.)}}{\partial r}\right)-\frac{u_r^{(.)}}{r^2}\right)+\mu\frac{1}{r^2}\frac{\partial^2 u_r^{(.)}}{\partial\theta^2}+(\lambda+\mu)\frac{1}{r}\frac{\partial^2 u_\theta^{(.)}}{\partial r\partial\theta}-(\lambda+3\mu)\frac{1}{r^2}\frac{\partial u_\theta^{(.)}}{\partial\theta}=\mu f_r^{(.)} \\ \mu\left(\frac{\partial^2 u_\theta^{(.)}}{\partial r^2}+\frac{1}{r}\frac{\partial u_\theta^{(.)}}{\partial r}-\frac{u_\theta^{(.)}}{r^2}\right)+(\lambda+2\mu)\frac{1}{r^2}\frac{\partial^2 u_\theta^{(.)}}{\partial\theta^2}+(\lambda+\mu)\frac{1}{r}\frac{\partial^2 u_r^{(.)}}{\partial r\partial\theta}+(\lambda+3\mu)\frac{1}{r^2}\frac{\partial u_r^{(.)}}{\partial\theta}=\mu f_\theta^{(.)} \end{array}\right. \tag{15}$$

where the symbol (.) should be replaced by $*$ or $p$. In addition $\boldsymbol{u}^W$ is any particular solution (without specifying specific boundary conditions) of:

$$\left\{\begin{array}{l} (\lambda+2\mu)\left(\frac{1}{\alpha^2}\left(\frac{\partial^2 u_r^{W}}{\partial r^2}+\frac{1}{r}\frac{\partial u_r^{W}}{\partial r}\right)-\frac{u_r^{W}}{r^2}\right)+\mu\frac{1}{r^2}\frac{\partial^2 u_r^{W}}{\partial\theta^2}+(\lambda+\mu)\frac{1}{r}\frac{\partial^2 u_\theta^{W}}{\partial r\partial\theta}-(\lambda+3\mu)\frac{1}{r^2}\frac{\partial u_\theta^{W}}{\partial\theta}=\rho g\sin(\theta) \\ \mu\left(\frac{\partial^2 u_\theta^{W}}{\partial r^2}+\frac{1}{r}\frac{\partial u_\theta^{W}}{\partial r}-\frac{u_\theta^{W}}{r^2}\right)+(\lambda+2\mu)\frac{1}{r^2}\frac{\partial^2 u_\theta^{W}}{\partial\theta^2}+(\lambda+\mu)\frac{1}{r}\frac{\partial^2 u_r^{W}}{\partial r\partial\theta}+(\lambda+3\mu)\frac{1}{r^2}\frac{\partial u_r^{W}}{\partial\theta}=\rho g\cos(\theta) \end{array}\right. \tag{16}$$

And finally $\widehat{\boldsymbol{u}}$ is the homogenous solution of the Navier equation:

$$\left\{\begin{array}{l} (\lambda+2\mu)\left(\frac{1}{\alpha^2}\left(\frac{\partial^2 \widehat{u}_r}{\partial r^2}+\frac{1}{r}\frac{\partial \widehat{u}_r}{\partial r}\right)-\frac{\widehat{u}_r}{r^2}\right)+\mu\frac{1}{r^2}\frac{\partial^2 \widehat{u}_r}{\partial\theta^2}+(\lambda+\mu)\frac{1}{r}\frac{\partial^2 \widehat{u}_\theta}{\partial r\partial\theta}-(\lambda+3\mu)\frac{1}{r^2}\frac{\partial \widehat{u}_\theta}{\partial\theta}=0 \\ \mu\left(\frac{\partial^2 \widehat{u}_\theta}{\partial r^2}+\frac{1}{r}\frac{\partial \widehat{u}_\theta}{\partial r}-\frac{\widehat{u}_\theta}{r^2}\right)+(\lambda+2\mu)\frac{1}{r^2}\frac{\partial^2 \widehat{u}_\theta}{\partial\theta^2}+(\lambda+\mu)\frac{1}{r}\frac{\partial^2 \widehat{u}_r}{\partial r\partial\theta}+(\lambda+3\mu)\frac{1}{r^2}\frac{\partial \widehat{u}_r}{\partial\theta}=0 \end{array}\right. \tag{17}$$

with boundary conditions:

$$\left\{\begin{array}{l} \left[\widehat{\boldsymbol{\sigma}}.\boldsymbol{n}\right](r_{sup},\theta)=T_r^{sup}(\theta)\boldsymbol{e}_r-\left[\left(\boldsymbol{\sigma}^*+\boldsymbol{\sigma}^p+\boldsymbol{\sigma}^W\right).\boldsymbol{n}\right](r_{sup},\theta)=\widehat{T}^{sup}(\theta) \\ \left[\widehat{\boldsymbol{\sigma}}.\boldsymbol{n}\right](r_{inf},\theta)=-\left[\left(\boldsymbol{\sigma}^*+\boldsymbol{\sigma}^p+\boldsymbol{\sigma}^W\right).\boldsymbol{n}\right](r_{inf},\theta)=\widehat{T}^{inf}(\theta) \end{array}\right. \tag{18}$$

This decomposition is summarized in figure 3.

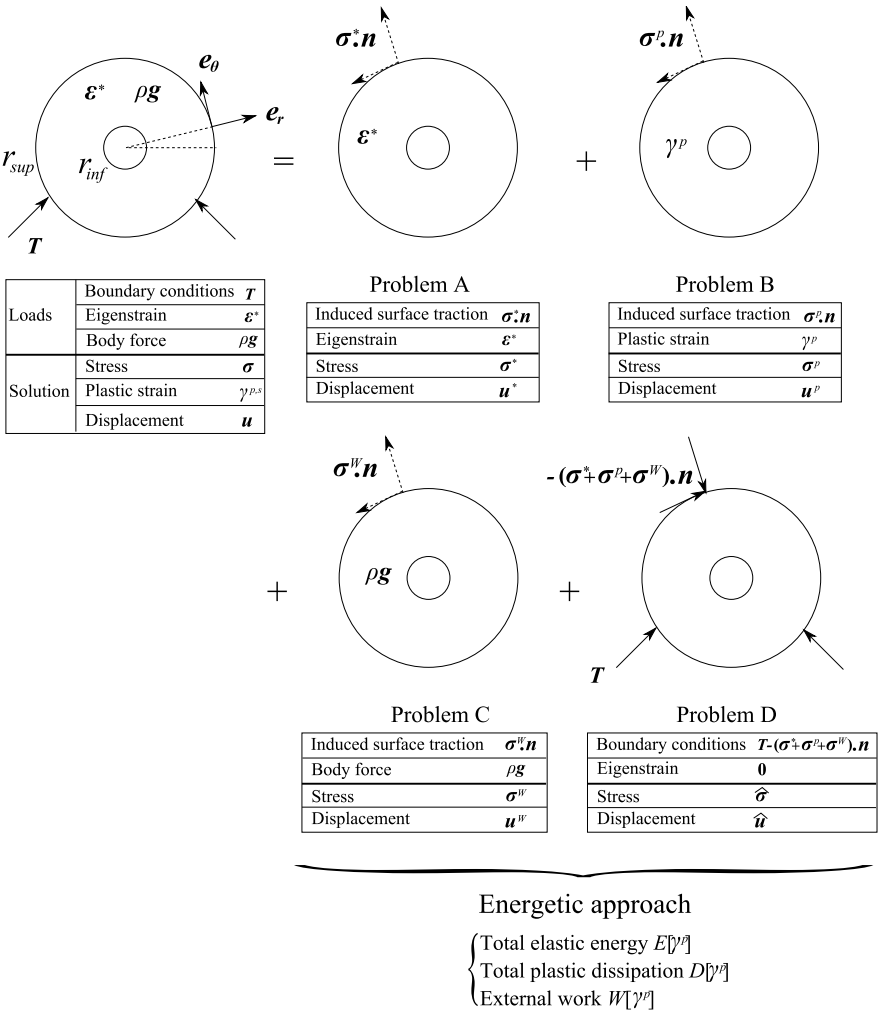


Figure 3: Decomposition and energetic principle

## 3. Mathematical preliminaries

This section deals with mathematical tools used in following sections. The analytical solution proposed in this paper relies on an orthogonal series expansion rather similar to the classic Fourier-Bessel series. Consider $J_\delta$ and $Y_\delta$ the Bessel functions of the $\delta$-order of the first and second kind respectively. Bessel functions are solutions of the following ordinary differential equation:

$$y''(x) + \frac{y'(x)}{x} + \left(1 - \frac{\delta^2}{x^2}\right) y(x) = 0 \tag{19}$$

In the following, an orthogonal function basis is introduced, so that any function $f : \left[r_{inf}, r_{sup}\right] \to \mathbb{C}$ can be approximated by projection on the corresponding vector space. This approach is an extension of the classical Fourier-Bessel series expansion. The proposed function basis is constructed from Bessel functions which are solutions of (19). The solution of the Navier equation (15) is projected on this orthogonal basis and terms of the form $y''(x) + \frac{y'(x)}{x} - \frac{\delta^2}{x^2} y(x)$ in the equation set is proportional to $y(x)$. The Navier equation (15) presents two terms of this form leading to terms proportional to $y(x)$. In addition, the right side term of

the Navier equation can also be projected and is proportional to $y(x)$. Therefore, the problem almost reduces to identify coefficients.

Consider normalized Bessel functions:

$$j_\delta(r) = \frac{J_\delta\left(\frac{r}{r_{sup}}\right)}{J_\delta\left(\frac{r_{inf}}{r_{sup}}\right)} \quad \text{and} \quad y_\delta(r) = \frac{Y_\delta\left(\frac{r}{r_{sup}}\right)}{Y_\delta\left(\frac{r_{inf}}{r_{sup}}\right)} \tag{20}$$

and the following function sequence:

$$G_m^{(\delta)}(r) = \frac{J_\delta\left(x_m^{(\delta)}\frac{r}{r_{sup}}\right)}{J_\delta\left(x_m^{(\delta)}\frac{r_{inf}}{r_{sup}}\right)} - \frac{Y_\delta\left(x_m^{(\delta)}\frac{r}{r_{sup}}\right)}{Y_\delta\left(x_m^{(\delta)}\frac{r_{inf}}{r_{sup}}\right)} \tag{21}$$

where $x_m^{(\delta)}$ are the successive positive roots (indexed by $1 \leq m \leq M$) of

$$x \mapsto J_\delta(x)\, Y_\delta\left(x\frac{r_{inf}}{r_{sup}}\right) - J_\delta\left(x\frac{r_{inf}}{r_{sup}}\right) Y_\delta(x) \tag{22}$$

Introducing the following scalar product:

$$\langle f, g\rangle = \int_{r_{inf}}^{r_{sup}} r f(r) g(r) \mathrm{d}r \tag{23}$$

one obtains the following orthogonality relations:

$$\left\langle G_m^{(\delta)}, G_l^{(\delta)}\right\rangle = \begin{cases} M_m^{(\delta)} & \text{if} \quad m = l \\ 0 & \text{if} \quad m \neq l \end{cases} \tag{24}$$

where $M_m^{(\delta)} \neq 0$ is defined as $\left\langle G_m^{(\delta)}, G_m^{(\delta)}\right\rangle$. The orthogonal series expansion consists in projecting any function $f : r \in \left[r_{inf}, r_{sup}\right] \to \mathbb{C}$ on the set of the function sequence $G_m^{(\delta)}$ defined by (21). However it should be noted that $G^{(\delta)}(r_{inf}) = G^{(\delta)}(r_{sup}) = 0$. Thus, it is very useful to project an auxiliary function that vanishes at $r = r_{sup}$ and $r = r_{inf}$, namely: $g(r) = f(r) - \left(F j_\delta(r) + \widetilde{F} y_\delta(r)\right)$ where:

$$\begin{pmatrix} F \\ \widetilde{F} \end{pmatrix} = \begin{pmatrix} 1 & 1 \\ j_\delta(r_{sup}) & y_\delta(r_{sup}) \end{pmatrix}^{-1} \cdot \begin{pmatrix} f(r_{inf}) \\ f(r_{sup}) \end{pmatrix} \tag{25}$$

Thus, any function $f : r \in \left[r_{inf}, r_{sup}\right] \to \mathbb{C}$ may be projected as follows:

$$f(r) = F j_\delta(r) + \widetilde{F} y_\delta(r) + \sum_{m=1}^{M} F_m G_m^{(\delta)}(r) \tag{26}$$

where the projection reads:

$$F_m = \frac{\left\langle G_m^{(\delta)}, f(r) - \left(F j_\delta(r) + \widetilde{F} y_\delta(r)\right)\right\rangle}{\left\langle G_m^{(\delta)}, G_m^{(\delta)}\right\rangle} \tag{27}$$

This projection procedure is repeatedly used on various functions in the following. For the sake of conciseness, equations (25) and (27) are not recalled each time.

It should be noted that roots $x_m$ are introduced similarly as for Fourier-Bessel series expansions, that is to say to generated an orthogonal function basis and not to verify specific boundary condition.

## 4. Particular non axi-symmetric solutions

The inhomogeneous Navier equations (15) are solved exactly the same way for $(f_r^*, f_\theta^*)$ and for $(f_r^p, f_\theta^p)$. Solutions $\boldsymbol{u}^*$ and $\boldsymbol{u}^p$ are presented separately for the sake of clarity because $\boldsymbol{\varepsilon}^*$ is an input of the model and $\gamma^p$ is a state variable that needs to be determined in the end by an optimization procedure, even though $\gamma^p$ is treated in this section as an imposed parametric eigenstrain. Solutions $\boldsymbol{u}^*$ and $\boldsymbol{u}^p$ are sought in the form of a Fourier series expansion:

$$\left\{ \begin{array}{l} u_r^{(.)} = \displaystyle\sum_{n=-N}^{N} u_n^{(r,.)}(r)\exp(in\theta) \quad u_\theta^{(.)} = \displaystyle\sum_{n=-N}^{N} u_n^{(\theta,.)}(r)\exp(in\theta) \end{array} \right. \tag{28}$$

where the symbol (.) should be replaced by $*$ or $p$. Right side terms of (15) are also expanded into Fourier series:

$$\left\{ \begin{array}{l} f_r^{(.)}(r,\theta) = \displaystyle\sum_{n=-N}^{N} f_n^{(r,.)}(r)\exp(in\theta) \\ f_\theta^{(.)}(r,\theta) = \displaystyle\sum_{n=-N}^{N} f_n^{(\theta,.)}(r)\exp(in\theta) \end{array} \right. \tag{29}$$

where $(r,.)$ and $(\theta,.)$ should be replaced by $(r,*)$ or $(r,p)$ and $(\theta,*)$ or $(\theta,p)$. Then, the inhomogeneous Navier equations (15) reduce to:

$$\left\{ \begin{array}{l} (\lambda+2\mu)\left(\dfrac{1}{\alpha^2}\left(\dfrac{\partial^2 u_n^{(r,.)}}{\partial r^2}+\dfrac{1}{r}\dfrac{\partial u_n^{(r,.)}}{\partial r}\right)-\dfrac{u_n^{(r,.)}}{r^2}\right)-n^2\mu\dfrac{u_n^{(r,.)}}{r^2}+in\left[(\lambda+\mu)\dfrac{1}{r}\dfrac{\partial u_n^{(\theta,.)}}{\partial r}-(\lambda+3\mu)\dfrac{u_n^{(\theta,.)}}{r^2}\right]=\mu f_n^{(r,.)}(r) \\ \mu\left(\dfrac{\partial^2 u_n^{(\theta,.)}}{\partial r^2}+\dfrac{1}{r}\dfrac{\partial u_n^{(\theta,.)}}{\partial r}-\dfrac{u_n^{(\theta,.)}}{r^2}\right)-n^2(\lambda+2\mu)\dfrac{u_n^{(\theta,.)}}{r^2}+in\left[(\lambda+\mu)\dfrac{1}{r}\dfrac{\partial u_n^{(r,.)}}{\partial r}+(\lambda+3\mu)\dfrac{u_n^{(r,.)}}{r^2}\right]=\mu f_n^{(\theta,.)(r)} \end{array} \right. \tag{30}$$

Consider:

$$\delta_n = \alpha\sqrt{1+\frac{\mu}{\lambda+2\mu}n^2} \;\Big|\; \zeta_n = \sqrt{1+\frac{\lambda+2\mu}{\mu}n^2} \tag{31}$$

One can rewrite (30):

$$\left\{ \begin{array}{l} \dfrac{\lambda+2\mu}{\alpha^2}\left(\dfrac{\partial^2 u_n^{(r,.)}}{\partial r^2}+\dfrac{1}{r}\dfrac{\partial u_n^{(r,.)}}{\partial r}-\dfrac{\delta_n^2}{r^2}u_n^{(r,.)}\right)+in\left[(\lambda+\mu)\dfrac{1}{r}\dfrac{\partial u_n^{(\theta,.)}}{\partial r}-(\lambda+3\mu)\dfrac{u_n^{(\theta,.)}}{r^2}\right]=\mu f_n^{(r,.)}(r) \\ \mu\left(\dfrac{\partial^2 u_n^{(\theta,.)}}{\partial r^2}+\dfrac{1}{r}\dfrac{\partial u_n^{(\theta,.)}}{\partial r}-\dfrac{\zeta_n^2}{r^2}u_n^{(\theta,.)}\right)+in\left[(\lambda+\mu)\dfrac{1}{r}\dfrac{\partial u_n^{(r,.)}}{\partial r}+(\lambda+3\mu)\dfrac{u_n^{(r,.)}}{r^2}\right]=\mu f_n^{(\theta,.)(r)} \end{array} \right. \tag{32}$$

The strategy is to make projections of $u_n^{(r,.)}(r)$ and $u_n^{(\theta,.)}(r)$ on the orthogonal basis related respectively to $\delta_n$ and $\zeta_n$, so that the first term of both equations in (32) are proportional to each term of the corresponding function basis (see (34)), as explained in section 3. Then, right side terms $f_n^{(r,.)}$ and $f_n^{(\theta,.)}$ are also projected on the function basis related respectively to $\delta_n$ and $\zeta_n$ (see (37)) as well as terms in brackets $in\,[...]$ (see (36)). Thus, the solution is obtained by coefficient identification.

More precisely, functions $u_n^{(r,.)}(r)$ and $u_n^{(\theta,.)}(r)$ are sought in the form:

$$\left\{ \begin{array}{l} u_n^{(r,.)}(r) = U_n^{(r,.)} j_{\delta_n}(r) + \widetilde{U}_n^{(r,.)} y_{\delta_n}(r) + \displaystyle\sum_{m=1}^{M} U_{m,n}^{(r,.)} G_m^{(\delta_n)}(r) \\ u_n^{(\theta,.)}(r) = U_n^{(\theta,.)} j_{\zeta_n}(r) + \widetilde{U}_n^{(\theta,.)} y_{\zeta_n}(r) + \displaystyle\sum_{m=1}^{M} U_{m,n}^{(\theta,.)} G_m^{(\zeta_n)}(r) \end{array} \right. \tag{33}$$

where $(r,.)$ and $(\theta,.)$ should be replaced by $(r,*)$ or $(r,p)$ and $(\theta,*)$ or $(\theta,p)$. From (19) and (33) one obtains:

$$\begin{cases} \dfrac{\lambda+2\mu}{\alpha^2}\left(\dfrac{\partial^2 u_n^{(r,.)}}{\partial r^2}+\dfrac{1}{r}\dfrac{\partial u_n^{(r,.)}}{\partial r}-\dfrac{\delta_n^2}{r^2}u_n^{(r,.)}\right)=-\dfrac{\lambda+2\mu}{\alpha^2 r_{sup}^2}\left(U_n^{(r,.)}j_{\delta_n}(r)+\widetilde{U}_n^{(r,.)}y_{\delta_n}(r)+\sum_{m=1}^{M}U_{m,n}^{(r,.)}\left(x_m^{(\delta_n)}\right)^2 G_m^{(\delta_n)}(r)\right) \\ \mu\left(\dfrac{\partial^2 u_n^{(\theta,.)}}{\partial r^2}+\dfrac{1}{r}\dfrac{\partial u_n^{(\theta,.)}}{\partial r}-\dfrac{\zeta_n^2}{r^2}u_n^{(\theta,.)}\right)=-\dfrac{\mu}{r_{sup}^2}\left(U_n^{(\theta,.)}j_{\zeta_n}(r)+\widetilde{U}_n^{(\theta,.)}y_{\zeta_n}(r)+\sum_{m=1}^{M}U_{m,n}^{(\theta,.)}\left(x_m^{(\zeta_n)}\right)^2 G_m^{(\zeta_n)}(r)\right) \end{cases} \tag{34}$$

Consider:

$$\begin{cases} h_n^{(r,.)}(r)=\dfrac{in}{\mu}\left[(\lambda+\mu)\dfrac{1}{r}\dfrac{\partial u_n^{(\theta,.)}}{\partial r}-(\lambda+3\mu)\dfrac{u_n^{(\theta,.)}}{r^2}\right] \\ h_n^{(\theta,.)}(r)=\dfrac{in}{\mu}\left[(\lambda+\mu)\dfrac{1}{r}\dfrac{\partial u_n^{(r,.)}}{\partial r}+(\lambda+3\mu)\dfrac{u_n^{(r,.)}}{r^2}\right] \end{cases} \tag{35}$$

Functions $h_n^{(r,.)}$ and $h_n^{(\theta,.)}$ are projected as follows:

$$\begin{cases} h_n^{(r,.)}(r)=H_n^{(r,.)}j_{\delta_n}(r)+\widetilde{H}_n^{(r,.)}y_{\delta_n}(r)+\sum_{m=1}^{M}H_{m,n}^{(r,.)}G^{(\delta_n)} \\ h_n^{(\theta,.)}(r)=H_n^{(\theta,.)}j_{\zeta_n}(r)+\widetilde{H}_n^{(\theta,.)}y_{\zeta_n}(r)+\sum_{m=1}^{M}H_{m,n}^{(\theta,.)}G^{(\zeta_n)} \end{cases} \tag{36}$$

where $H_n^{(r,.)}$, $\widetilde{H}_n^{(r,.)}$ and $H_{m,n}^{(r,.)}$ are explicitly defined as functions of $U_n^{(\theta,.)}$, $\widetilde{U}_n^{(\theta,.)}$ and $U_{l,n}^{(\theta,.)}$ and where $H_n^{(\theta,.)}$, $\widetilde{H}_n^{(\theta,.)}$ and $H_{m,n}^{(\theta,.)}$ are explicitly defined as functions of $U_n^{(r,.)}$, $\widetilde{U}_n^{(r,.)}$ and $U_{l,n}^{(r,.)}$. Functions $f_n^{(r,.)}$ and $f_n^{(\theta,.)}$ are projected as follows:

$$\begin{cases} f_n^{(r,.)}=F_n^{(r,.)}j_{\delta_n}(r)+\widetilde{F}_n^{(r,.)}y_{\delta_n}(r)+\sum_{m=1}^{M}F_{m,n}^{(r,.)}G^{(\delta_n)} \\ f_n^{(\theta,.)}=F_n^{(\theta,.)}j_{\zeta_n}(r)+\widetilde{F}_n^{(\theta,.)}y_{\zeta_n}(r)+\sum_{m=1}^{M}F_{m,n}^{(\theta,.)}G^{(\zeta_n)} \end{cases} \tag{37}$$

Hence:

$$\begin{array}{l|l} -\dfrac{\lambda+2\mu}{\mu\alpha^2 r_{sup}^2}U_n^{(r,.)}+H_n^{(r,.)}=F_n^{(r,.)} & -\dfrac{1}{r_{sup}^2}U_n^{(\theta,.)}+H_n^{(\theta,.)}=F_n^{(\theta,.)} \\ -\dfrac{\lambda+2\mu}{\mu\alpha^2 r_{sup}^2}\widetilde{U}_n^{(r,.)}+\widetilde{H}_n^{(r,.)}=\widetilde{F}_n^{(r,.)} & -\dfrac{1}{r_{sup}^2}\widetilde{U}_n^{(\theta,.)}+\widetilde{H}_n^{(\theta,.)}=\widetilde{F}_n^{(\theta,.)} \\ -\dfrac{\left(x_m^{(\delta_n)}\right)^2(\lambda+2\mu)}{\mu\alpha^2 r_{sup}^2}U_{m,n}^{(r,.)}+H_{m,n}^{(r,.)}=F_{m,n}^{(r,.)} & -\dfrac{\left(x_m^{(\zeta_n)}\right)^2}{r_{sup}^2}U_{m,n}^{(\theta,.)}+H_{m,n}^{(\theta,.)}=F_{m,n}^{(\theta,.)} \end{array} \tag{38}$$

These equations may be written in matrix form and solved as follows:

$$\boldsymbol{U}_n^{(.)}=[\boldsymbol{S}_n]^{-1}.\boldsymbol{F}_n^{(.)} \tag{39}$$

where:

$$\begin{cases} \boldsymbol{U}_n^{(.)}=\left(U_n^{(r,.)},\widetilde{U}_n^{(r,.)},U_{1,n}^{(r,.)},\cdots,U_{M,n}^{(r,.)},U_n^{(\theta,.)},\widetilde{U}_n^{(\theta,.)},U_{1,n}^{(\theta,.)},\cdots,U_{M,n}^{(\theta,.)}\right)^T \\ \boldsymbol{F}_n^{(.)}=\left(F_n^{(r,.)},\widetilde{F}_n^{(r,.)},F_{1,n}^{(r,.)},\cdots,F_{M,n}^{(r,.)},F_n^{(\theta,.)},\widetilde{F}_n^{(\theta,.)},F_{1,n}^{(\theta,.)},\cdots,F_{M,n}^{(\theta,.)}\right)^T \end{cases} \tag{40}$$

and where:

$$\boldsymbol{S}_n = \begin{pmatrix} -\frac{\lambda+2\mu}{\mu\alpha^2} \times \boldsymbol{I}_r & \boldsymbol{s_r} \\ \boldsymbol{s_\theta} & -\boldsymbol{I}_\theta \end{pmatrix} \tag{41}$$

where $\boldsymbol{I}_r$ and $\boldsymbol{I}_\theta$ denote diagonal matrices of size $(M+2)\times(M+2)$ with respective diagonals $1/r_{sup}^2\left(1,1,\left(x_1^{(\delta_n)}\right)^2,\cdots,\left(x_M^{(\delta_n)}\right)^2\right)$ and $1/r_{sup}\left(1,1,\left(x_1^{(\zeta_n)}\right)^2,\cdots,\left(x_M^{(\zeta_n)}\right)^2\right)$. Moreover $\boldsymbol{s_r}$ and $\boldsymbol{s_\theta}$ denote matrices of size $(M+2)\times(M+2)$ defined by (38). The stress tensors reads:

$$\begin{cases} \sigma_{rr}^* = \dfrac{\lambda+2\mu}{\alpha^2}\left(\dfrac{\partial u_r^*}{\partial r} - \varepsilon_{rr}^*\right) + \lambda\left(\dfrac{u_r^*}{r} + \dfrac{1}{r}\dfrac{\partial u_\theta^*}{\partial\theta} - \varepsilon_{\theta\theta}^*\right) \\ \sigma_{\theta\theta}^* = (\lambda+2\mu)\left(\dfrac{u_r^*}{r} + \dfrac{1}{r}\dfrac{\partial u_\theta^*}{\partial\theta} - \varepsilon_{\theta\theta}^*\right) + \lambda\left(\dfrac{\partial u_r^*}{\partial r} - \varepsilon_{rr}^*\right) \\ \sigma_{r\theta}^* = \mu\left(\dfrac{1}{r}\dfrac{\partial u_r^*}{\partial\theta} + \dfrac{\partial u_\theta^*}{\partial r} - \dfrac{u_\theta^*}{r} - 2\varepsilon_{r\theta}^*\right) \end{cases} \tag{42}$$

and:

$$\begin{cases} \sigma_{rr}^p = \dfrac{\lambda+2\mu}{\alpha^2}\dfrac{\partial u_r^p}{\partial r} + \lambda\left(\dfrac{u_r^p}{r} + \dfrac{1}{r}\dfrac{\partial u_\theta^p}{\partial\theta}\right) \\ \sigma_{\theta\theta}^p = (\lambda+2\mu)\left(\dfrac{u_r^p}{r} + \dfrac{1}{r}\dfrac{\partial u_\theta^p}{\partial\theta}\right) + \lambda\dfrac{\partial u_r^p}{\partial r} \\ \sigma_{r\theta}^p = \mu\left(\dfrac{1}{r}\dfrac{\partial u_r^p}{\partial\theta} + \dfrac{\partial u_\theta^p}{\partial r} - \dfrac{u_\theta^p}{r} - \gamma_{r\theta}^p\right) \end{cases} \tag{43}$$

A particular solution of the Navier equation (16) accounting for gravity (without specifying specific boundary conditions) can be derived exactly the same way as the particular solution of the Navier equations (15). Since the right side term of (16) only involves sine and cosine functions the procedure detailed above is limited to $n=1$ and $n=-1$. However, if $\lambda\neq\mu$ (i.e., if the Poisson coefficient $\nu\neq 0.25$) then a very simple particular solution of (16) can be obtained. Displacements $u_r^W$ and $u_\theta^W$ read:

$$\text{if } \lambda\neq\mu,\ \begin{cases} u_r^W = 0 \\ u_\theta^W = -\dfrac{\rho g}{\lambda-\mu}r^2\cos(\theta) \end{cases} \tag{44}$$

Hence:

$$\text{if } \lambda\neq\mu,\ \begin{cases} \sigma_{rr}^W = \rho g\dfrac{\lambda}{\lambda-\mu}r\sin(\theta) \\ \sigma_{\theta\theta}^W = \rho g\dfrac{\lambda+2\mu}{\lambda-\mu}r\sin(\theta) \\ \sigma_{r\theta}^W = -\rho g\dfrac{\mu}{\lambda-\mu}r\cos(\theta) \end{cases} \tag{45}$$

Of course the resultant force at both boundaries is equal to the opposite of the total weight.

It should be noted that the resultant force at the inner surface $r=r_{inf}$ does not vanish. This is due to the fact that particular solutions of the Navier equation have been derived without imposing specific boundary conditions. The homogenous solution derived in section 5 enables us to impose boundary conditions so that the total solution defined by (14) verify the prescribed boundary conditions. In particular normal stress vanishes at the inner radius.

## 5. Homogenous solution with boundary conditions

The homogenous Navier equation (17) with boundary conditions (18) is solved in this section. A Fourier series expansion is considered:

$$\begin{cases} \widehat{u_r}(r,\theta) = \displaystyle\sum_{n=-N}^{N} \widehat{u}_n^{(r)}(r)\exp(in\theta) \\ \widehat{u_\theta}(r,\theta) = \displaystyle\sum_{n=-N}^{N} \widehat{u}_n^{(\theta)}(r)\exp(in\theta) \end{cases} \tag{46}$$

The homogenous Navier equation (17) reduces to:

$$\begin{cases} (\lambda+2\mu)\left(\dfrac{1}{\alpha^2}\left(\dfrac{\partial^2\widehat{u}_n^{(r)}}{\partial r^2}+\dfrac{1}{r}\dfrac{\partial\widehat{u}_n^{(r)}}{\partial r}\right)-\dfrac{\widehat{u}_n^{(r)}}{r^2}\right)-n^2\mu\dfrac{\widehat{u}_n^{(r)}}{r^2}+in\left[(\lambda+\mu)\dfrac{1}{r}\dfrac{\partial\widehat{u}_n^{(\theta)}}{\partial r}-(\lambda+3\mu)\dfrac{\widehat{u}_n^{(\theta)}}{r^2}\right]=0 \\ \mu\left(\dfrac{\partial^2\widehat{u}_n^{(\theta)}}{\partial r^2}+\dfrac{1}{r}\dfrac{\partial\widehat{u}_n^{(\theta)}}{\partial r}-\dfrac{\widehat{u}_n^{(\theta)}}{r^2}\right)-n^2(\lambda+2\mu)\dfrac{\widehat{u}_n^{(\theta)}}{r^2}+in\left[(\lambda+\mu)\dfrac{1}{r}\dfrac{\partial\widehat{u}_n^{(r)}}{\partial r}+(\lambda+3\mu)\dfrac{\widehat{u}_n^{(r)}}{r^2}\right]=0 \end{cases} \tag{47}$$

The orthogonal function basis proposed in section 3 cannot be used anymore as the right side term is zero. Indeed, the use of the orthogonal function basis leads to (39), which gives a zero solution if the right side term $\boldsymbol{F}_n^{(.)}$ vanishes. As the equation set (47) consists in two coupled second-order partial differential equations the space of homogenous solutions is four-dimensional. Displacements are sought proportional to $r^\beta$ with $\beta = \beta_R + i\beta_I \in \mathbb{C}$, where:

$$r^\beta = r^{\beta_R}\left(\cos\left(\beta_I\log(r)\right) + i\sin\left(\beta_I\log(r)\right)\right) \tag{48}$$

That is to say that displacements are sought in the form $\widehat{u}_n^{(r)} = ar^\beta$ and $\widehat{u}_n^{(\theta)} = br^\beta$. Introducing this form into (47) one obtains:

$$\underbrace{\begin{pmatrix} (\lambda+2\mu)\left(\dfrac{\beta^2}{\alpha^2}-1\right)-n^2\mu & in\left[(\lambda+\mu)\beta-(\lambda+3\mu)\right] \\ in\left[(\lambda+\mu)\beta+\lambda+3\mu\right] & \mu\left(\beta^2-1\right)-n^2(\lambda+2\mu) \end{pmatrix}}_{\boldsymbol{M}_n(\beta)} \cdot \begin{pmatrix} a \\ b \end{pmatrix} = \begin{pmatrix} 0 \\ 0 \end{pmatrix} \tag{49}$$

Hence, non-zero solutions are obtained if $\det\left[\boldsymbol{M}_n(\beta)\right] = 0$. This equation is called the characteristic equation and reduces to:

$$\beta^4 + \left(\alpha^2\frac{\lambda n^2-\mu}{\mu} - \frac{\lambda+2\mu}{\mu}n^2 - 1\right)\beta^2 + \alpha^2(n^2-1)^2 = 0 \tag{50}$$

If $\beta$ is solution of (50) then the first equation in (49) can be discarded and:

$$\forall n \geq 1,\ \frac{a}{b} = -\frac{\mu(\beta^2-1)-n^2(\lambda+2\mu)}{in\left[(\lambda+\mu)\beta+\lambda+3\mu\right]} \tag{51}$$

If $n = 0$, there is no constrain on $a$ and $b$.

There are four solutions of (50) in $\mathbb{C}$, denoted by $\boldsymbol{\beta}_n = (\beta_{n,1}, \beta_{n,2}, \beta_{n,3}, \beta_{n,4})$, which corresponds to the fact that the solution space should be four-dimensional. Finally the homogenous

solution is written as a linear combination of the four solutions defined by $\beta_{n,k}$ ($1 \leq k \leq 4$) and reads for $n \geq 2$:

$$\begin{cases} \widehat{u}_n^{(r)}(r) = \displaystyle\sum_{k=1}^{4} \widehat{u}_{n,k} a_{n,k} \left(\frac{r}{r_{sup}}\right)^{\beta_{n,k}} \exp(in\theta) \\ \widehat{u}_n^{(\theta)}(r) = \displaystyle\sum_{k=1}^{4} \widehat{u}_{n,k} b_{n,k} \left(\frac{r}{r_{sup}}\right)^{\beta_{n,k}} \exp(in\theta) \end{cases} \tag{52}$$

where $\widehat{\boldsymbol{u}}_n = (\widehat{u}_{n,1}, \widehat{u}_{n,2}, \widehat{u}_{n,3}, \widehat{u}_{n,4})$ and similarly $\boldsymbol{a}_n$ and $\boldsymbol{b}_n$ are defined such as:

$$n \geq 1, \begin{cases} a_{n,k} = (\beta_{n,k}^2 - 1) - n^2 \dfrac{\lambda + 2\mu}{\mu} \\ b_{n,k} = -in\left(\dfrac{\lambda + \mu}{\mu}\beta_{n,k} + \dfrac{\lambda + 3\mu}{\mu}\right) \end{cases} \tag{53}$$

For $n = 0$, one obtains $\boldsymbol{\beta}_0 = (1, -1, \alpha, -\alpha)$. So $\beta = 1$ is solution of the characteristic equation (50). For $n = 0$ and $\beta = 1$, (49) reduces to:

$$\begin{pmatrix} (\lambda + 2\mu)\left(\dfrac{1}{\alpha^2} - 1\right) & 0 \\ 0 & 0 \end{pmatrix} \cdot \begin{pmatrix} a \\ b \end{pmatrix} = \begin{pmatrix} 0 \\ 0 \end{pmatrix} \Rightarrow a = 0 \text{ and } b \in \mathbb{R} \tag{54}$$

Thus, for $n = 0$ and $\beta = 1$, the homogenous solution of (47) is $\widehat{u}_0^{(r)} = 0$ and $\widehat{u}_0^{(\theta)} = br$, which corresponds to a rigid rotation and should therefore be discarded. Thus, there is only three unknowns for $n = 0$ corresponding to $\beta = -1, \alpha, -\alpha$ and:

$$\begin{cases} \widehat{u}_0^{(r)}(r) = \widehat{u}_{0,1}\left(\dfrac{r}{r_{sup}}\right)^{-\alpha} + \widehat{u}_{0,2}\left(\dfrac{r}{r_{sup}}\right)^{\alpha} \\ \widehat{u}_0^{(\theta)}(r) = \widehat{u}_{0,3}\left(\dfrac{r}{r_{sup}}\right)^{-1} \end{cases} \tag{55}$$

For $n = 1$, one obtains $\boldsymbol{\beta}_1 = (0, 0, \beta_{1,1}, \beta_{1,2})$, thus $\beta = 0$ is a double root of the characteristic equation (50). For $n = 1$ and $\beta = 0$, (49) reduces to:

$$-(\lambda + 3\mu)\begin{pmatrix} 1 & i \\ -i & 1 \end{pmatrix} \cdot \begin{pmatrix} a \\ b \end{pmatrix} = \begin{pmatrix} 0 \\ 0 \end{pmatrix} \Rightarrow b = ia \in \mathbb{C} \tag{56}$$

Thus, for $n = 1$ and $\beta = 0$, the homogenous solution of (47) is $\widehat{u}_1^{(r)} = a$ and $\widehat{u}_1^{(\theta)} = ia$. Moreover displacements in the Cartesian coordinates read:

$$\begin{cases} \widehat{u}_x = \widehat{u}_r \cos(\theta) - \widehat{u}_\theta \sin(\theta) \\ \widehat{u}_y = \widehat{u}_r \sin(\theta) + \widehat{u}_\theta \cos(\theta) \end{cases} \tag{57}$$

In addition, if $n = 1$ and $n = -1$ are the only terms in Fourier expansion, then:

$$\begin{cases} \widehat{u}_r = 2\mathrm{Re}\left[\widehat{u}_1^{(r)} \exp(i\theta)\right] = 2(a_R \cos(\theta) - a_I \sin(\theta)) \\ \widehat{u}_\theta = 2\mathrm{Re}\left[\widehat{u}_1^{(\theta)} \exp(i\theta)\right] = -2(a_R \sin(\theta) + a_I \cos(\theta)) \end{cases} \tag{58}$$

where $a = a_R + ia_I$. Combining (57) and (58) one obtains:

$$\begin{cases} \widehat{u}_x = 2a_R \\ \widehat{u}_y = -2a_I \end{cases} \tag{59}$$

Thus, for $n = 1$ and $\beta = 0$ the solution corresponds to a rigid translation and should therefore be discarded. Since $\beta = 0$ is a double root of the characteristic equation (50), only two unknowns remain for $n = 1$ (corresponding to $\beta = \beta_{1,1}, \beta_{1,2}$). However, the resultant force applied at the inner radius $r_{inf}$ does not vanish (even though a global equilibrium is ensured) because of the particular solutions derived in section 4. Classically, a logarithmic solution of the form $\widehat{u}_1^{(r)} = a \log\left(r/r_{sup}\right) + c$ and $\widehat{u}_1^{(\theta)} = b \log\left(r/r_{sup}\right) + d$ should be introduced, leading to a third unknown. By introducing this form into (47) one can identify $a, b, c, d$. Therefore for $n = 1$:

$$\begin{cases} \widehat{u}_1^{(r)}(r) = \left[\displaystyle\sum_{k=1}^{2} \widehat{u}_{1,k} a_{1,k} \left(\frac{r}{r_{sup}}\right)^{\beta_{1,k}} + \widehat{u}_{1,3} \left(\log\left(\frac{r}{r_{sup}}\right) - \frac{\lambda+\mu}{\lambda+3\mu}\right)\right] \exp(i\theta) \\ \widehat{u}_1^{(\theta)}(r) = \left[\displaystyle\sum_{k=1}^{2} \widehat{u}_{1,k} b_{1,k} \left(\frac{r}{r_{sup}}\right)^{\beta_{1,k}} + i\,\widehat{u}_{1,3} \log\left(\frac{r}{r_{sup}}\right)\right] \exp(i\theta) \end{cases} \tag{60}$$

It should be noted that displacements for $-n$ (with $n \geq 1$) are simply conjugates of those for $n$.

Boundary conditions (18) are considered. A Fourier series expansion is needed.

$$T_r^{sup}(\theta) = \sum_{n=-N}^{N} T_n^{(r,sup)} \exp(in\theta) \tag{61}$$

where:

$$T_n^{(r,sup)} = \frac{1}{2\pi} \int_0^{2\pi} T_r^{sup}(\theta) \exp(-in\theta) \mathrm{d}\theta \tag{62}$$

Hence:

$$T_n^{(r,sup)} = \frac{\left(r_{sup}^2 - r_{inf}^2\right)\rho g}{4 \sin(\theta_0) r_{sup}} \left(\exp(-in\theta_0) + (-1)^n \exp(in\theta_0)\right) \tag{63}$$

Moreover $(\widehat{T}_r^{sup}, \widehat{T}_\theta^{sup}, \widehat{T}_r^{inf}, \widehat{T}_\theta^{inf})$ are also expanded into a Fourier series:

$$\begin{cases} \widehat{T}_{(.)}^{sup}(\theta) = \displaystyle\sum_{n=-N}^{N} \widehat{T}_n^{(.,sup)} \exp(in\theta) \\ \widehat{T}_{(.)}^{inf}(\theta) = \displaystyle\sum_{n=-N}^{N} \widehat{T}_n^{(.,inf)} \exp(in\theta) \end{cases} \tag{64}$$

where (.) stands for $r$ or $\theta$. Fourier coefficients are denoted by $(\widehat{T}_n^{(r,sup)}, \widehat{T}_n^{(\theta,sup)}, \widehat{T}_n^{(r,inf)}, \widehat{T}_n^{(\theta,inf)})$. The stress tensor reads:

$$\begin{cases} \widehat{\sigma}_{rr} = \dfrac{\lambda+2\mu}{\alpha^2} \dfrac{\partial \widehat{u}_r}{\partial r} + \lambda \left(\dfrac{\widehat{u}_r}{r} + \dfrac{1}{r} \dfrac{\partial \widehat{u}_\theta}{\partial \theta}\right) \\ \widehat{\sigma}_{\theta\theta} = (\lambda+2\mu) \left(\dfrac{\widehat{u}_r}{r} + \dfrac{1}{r} \dfrac{\partial \widehat{u}_\theta}{\partial \theta}\right) + \lambda \dfrac{\partial \widehat{u}_r}{\partial r} \\ \widehat{\sigma}_{r\theta} = \mu \left(\dfrac{1}{r} \dfrac{\partial \widehat{u}_r}{\partial \theta} + \dfrac{\partial \widehat{u}_\theta}{\partial r} - \dfrac{\widehat{u}_\theta}{r}\right) \end{cases} \tag{65}$$

For all $n \geq 2$, there are 4 unknown coefficients $\widehat{\boldsymbol{u}}_n$ and 4 boundary conditions (involving $\widehat{\sigma}_{rr}$ and $\widehat{\sigma}_{r\theta}$ at $r = r_{sup}$ and at $r = r_{inf}$). Therefore by using the boundary condition (18) along with (65)

and (52) one obtains the following coefficients:

$$\forall n \geq 2$$

$$\frac{1}{r_{sup}}\begin{pmatrix} M_{n,1}^{(r)} & M_{n,2}^{(r)} & M_{n,3}^{(r)} & M_{n,4}^{(r)} \\ M_{n,1}^{(\theta)} & M_{n,2}^{(\theta)} & M_{n,3}^{(\theta)} & M_{n,4}^{(\theta)} \\ M_{n,1}^{(r)}\left(\frac{r_{inf}}{r_{sup}}\right)^{\beta_{1,1}-1} & M_{n,2}^{(r)}\left(\frac{r_{inf}}{r_{sup}}\right)^{\beta_{1,2}-1} & M_{n,3}^{(r)}\left(\frac{r_{inf}}{r_{sup}}\right)^{\beta_{1,3}-1} & M_{n,4}^{(r)}\left(\frac{r_{inf}}{r_{sup}}\right)^{\beta_{1,4}-1} \\ M_{n,1}^{(\theta)}\left(\frac{r_{inf}}{r_{sup}}\right)^{\beta_{1,1}-1} & M_{n,2}^{(\theta)}\left(\frac{r_{inf}}{r_{sup}}\right)^{\beta_{1,2}-1} & M_{n,3}^{(\theta)}\left(\frac{r_{inf}}{r_{sup}}\right)^{\beta_{1,3}-1} & M_{n,4}^{(\theta)}\left(\frac{r_{inf}}{r_{sup}}\right)^{\beta_{1,4}-1} \end{pmatrix} \cdot \begin{pmatrix} \widehat{u}_{n,1} \\ \widehat{u}_{n,2} \\ \widehat{u}_{n,3} \\ \widehat{u}_{n,4} \end{pmatrix} = \begin{pmatrix} \widehat{T}_n^{(r,sup)} \\ \widehat{T}_n^{(\theta,sup)} \\ \widehat{T}_n^{(r,inf)} \\ \widehat{T}_n^{(\theta,inf)} \end{pmatrix} \tag{66}$$

where:

$$M_{n,k}^{(r)} = a_{n,k}\left(\frac{\lambda+2\mu}{\alpha^2}\beta_{n,k}+\lambda\right)+i\lambda b_{n,k} \quad \Big| \quad M_{n,k}^{(\theta)} = \mu\left[ia_{n,k}+b_{n,k}\left(\beta_{n,k}-1\right)\right] \tag{67}$$

However, as already mentioned there is only three unknowns for $n = 1$, which is consistent with the reduction of boundary conditions due to the global resultant force equilibrium that reads:

$$r_{sup}\widehat{T}_1^{(r,sup)} - r_{inf}\widehat{T}_1^{(r,inf)} = i\left(r_{sup}\widehat{T}_1^{(\theta,sup)} - r_{inf}\widehat{T}_1^{(\theta,inf)}\right) \tag{68}$$

Hence for $n = 1$:

$$\frac{1}{r_{sup}}\begin{pmatrix} M_{1,1}^{(r)} & M_{1,2}^{(r)} & \frac{\lambda+2\mu}{\alpha^2}-\frac{\lambda(\lambda+\mu)}{\lambda+3\mu} \\ M_{1,1}^{(\theta)} & M_{1,2}^{(\theta)} & \frac{2\mu^2 i}{\lambda+3\mu} \\ M_{1,1}^{(r)}\left(\frac{r_{inf}}{r_{sup}}\right)^{\beta_{1,1}-1} & M_{1,2}^{(r)}\left(\frac{r_{inf}}{r_{sup}}\right)^{\beta_{1,2}-1} & \left(\frac{\lambda+2\mu}{\alpha^2}-\frac{\lambda(\lambda+\mu)}{\lambda+3\mu}\right)\frac{r_{sup}}{r_{inf}} \end{pmatrix} \cdot \begin{pmatrix} \widehat{u}_{1,1} \\ \widehat{u}_{1,2} \\ \widehat{u}_{1,3} \end{pmatrix} = \begin{pmatrix} \widehat{T}_1^{(r,sup)} \\ \widehat{T}_1^{(\theta,sup)} \\ \widehat{T}_1^{(r,inf)} \end{pmatrix} \tag{69}$$

It should be noted that the last equation corresponding to $\widehat{T}_1^{(\theta,inf)}$ is automatically verified. Similarly, for $n = 0$ there are only three unknowns which is consistent with the global momentum equilibrium that reads:

$$r_{sup}^2\widehat{T}_0^{(\theta,sup)} = r_{inf}^2\widehat{T}_0^{(\theta,inf)} \tag{70}$$

Hence for $n = 0$:

$$\frac{1}{r_{sup}}\begin{pmatrix} \left(\lambda-\frac{\lambda+2\mu}{\alpha}\right) & \left(\lambda+\frac{\lambda+2\mu}{\alpha}\right) \\ \left(\lambda-\frac{\lambda+2\mu}{\alpha}\right)\left(\frac{r_{inf}}{r_{sup}}\right)^{-(\alpha+1)} & \left(\lambda+\frac{\lambda+2\mu}{\alpha}\right)\left(\frac{r_{inf}}{r_{sup}}\right)^{\alpha-1} \end{pmatrix} \cdot \begin{pmatrix} \widehat{u}_{0,1} \\ \widehat{u}_{0,2} \end{pmatrix} = \begin{pmatrix} \widehat{T}_0^{(r,sup)} \\ \widehat{T}_0^{(r,inf)} \end{pmatrix} \tag{71}$$

and:

$$\widehat{u}_{0,3} = -r_{sup}\frac{\widehat{T}_0^{(\theta,sup)}}{2\mu} \tag{72}$$

## 6. Energetic approach

The analytical solution derived in previous sections relies on arbitrary parametric plastic-like shear strain $\gamma^p$. As already mentioned, for any arbitrary $\gamma^p$, a linear problem has been solved. In this section, all non-linear aspects are handled through an energetic approach. The proposed solution consists in determining the plastic-like shear strain so that the total energy is minimized by a quasi-Newton algorithm. In order to perform the minimization on a finite dimension space, functions $\gamma^p$ are sought in the following parametrized form:

$$\gamma^p(r,\theta) = \sum_{n=-N}^{N} \gamma_n^p(r)\exp(in\theta) \tag{73}$$

where:

$$\gamma_n^p(r) = \gamma_n j_0(r) + \widetilde{\gamma}_n y_0(r) + \sum_{m=1}^{M} \gamma_{m,n} G_m^{(0)}(r) \tag{74}$$

Consider the following parameter space of dimension $(M+2)$ for ($-N \leq n \leq N$ with $n \neq 0$):

$$\mathcal{P}_n = \left\{ (\gamma_n, \widetilde{\gamma}_n, \gamma_{1,n}, \cdots, \gamma_{M,n}) \in \mathbb{C}^{M+2} \right\} \tag{75}$$

Thus, the minimization is done on the following Cartesian product space of dimension $2N(M+2)$:

$$\mathcal{P} = \prod_{\substack{-N \leq n \leq N \\ n \neq 0}} \mathcal{P}_n \tag{76}$$

For any parameter vector $\boldsymbol{P} \in \mathcal{P}$ the elastic bulk energy $E[\boldsymbol{P}]$ is given by:

$$E[\boldsymbol{P}] = \frac{1}{2} \int_\Omega \boldsymbol{\sigma}[\boldsymbol{P}] : \boldsymbol{\varepsilon}[\boldsymbol{P}] \, \mathrm{d}\Omega \tag{77}$$

The work of external forces $W[\boldsymbol{P}]$ reads:

$$W[\boldsymbol{P}] = \int_{\partial\Omega} \boldsymbol{T}.\boldsymbol{u}[\boldsymbol{P}] \, \mathrm{d}S - \int_\Omega \rho g \boldsymbol{e}_y.\boldsymbol{u}[\boldsymbol{P}] \, \mathrm{d}\Omega \tag{78}$$

The plastic-like dissipated energy $D[\boldsymbol{P}]$ reads:

$$D[\boldsymbol{P}] = \int_\Omega \sigma_C \gamma_{cum}^p[\boldsymbol{P}] \, \mathrm{d}\Omega \tag{79}$$

where $\sigma_C$ is the critical shear stress that should be understood as a shear threshold. In addition, $\gamma_{cum}^p$ is the cumulative plastic-like shear strain defined by:

$$\gamma_{cum}^p[\boldsymbol{P}] = \sqrt{\frac{1}{3}} |\gamma^p| \tag{80}$$

In this contribution, a simplified expression of $\sigma_C$ is derived in Appendix B:

$$\sigma_C = \sqrt{3} f_C P_C \tag{81}$$

where $f_C$ is a friction coefficient (depending on lubrication conditions and roughness) and $P_C$ is the averaged contact pressure. The following minimum procedure holds:

$$\boldsymbol{P}^S = \underset{\boldsymbol{P} \in \mathcal{P}}{\operatorname{argmin}} \left( E[\boldsymbol{P}] - W[\boldsymbol{P}] + D[\boldsymbol{P}] \right) \tag{82}$$

Since the proposed solution relies on an analytical computation, the gradient of the total energy is easily computed for any parameter vector $\boldsymbol{P} \in \mathcal{P}$. This enables us to use fast quasi-Newton optimization algorithms for the minimization.

$$\begin{cases} \dfrac{\partial E[\boldsymbol{P}]}{\partial P_j} = \displaystyle\int_\Omega \boldsymbol{\varepsilon}[\boldsymbol{P}] : \boldsymbol{C} : \frac{\partial \boldsymbol{\varepsilon}[\boldsymbol{P}]}{\partial P_j} \mathrm{d}\Omega \\ \dfrac{\partial W[\boldsymbol{P}]}{\partial P_j} = \displaystyle\int_{\partial\Omega} \boldsymbol{T}.\frac{\partial \boldsymbol{u}[\boldsymbol{P}]}{\partial P_j} \mathrm{d}S \\ \dfrac{\partial D[\boldsymbol{P}]}{\partial P_j} = \displaystyle\int_{\partial\Omega} \sigma_C \, \frac{\partial \gamma_{cum}^p[\boldsymbol{P}]}{\partial P_j} \mathrm{d}S \end{cases} \tag{83}$$

The gradient (83) is computed as follows. From (39) one obtains the following gradient:

$$\frac{\partial \boldsymbol{U}_n^p}{\partial P_j} = [\boldsymbol{S}_n]^{-1} . \frac{\partial \boldsymbol{F}_n^p}{\partial P_j} \tag{84}$$

where $P_j$ may be $\gamma_n$, $\widetilde{\gamma}_n$ or $\gamma_{m,n}$. From (84) one can easily evaluate (83). This gradient necessitates to compute the partial derivatives of $\boldsymbol{F}_n^p$. The right side term $f_n^{(r,p)}, f_n^{(\theta,p)}$ is defined by (13) and $\gamma_n^p(r)$ is defined by (74). Thus, the projection $\boldsymbol{F}_n^p$ given by (37) may be computed by using the following projections on the set of functions used for the minimization procedure:

$$\begin{cases} \dfrac{in j_0(r)}{r} = C_n^{(j)} j_{\delta_n}(r) + \widetilde{C}_n^{(j)} y_{\delta_n}(r) + \displaystyle\sum_{k=1}^{M} C_{k,n}^{(j)} G_k^{(\delta_n)}(r) \\ \dfrac{in y_0(r)}{r} = C_n^{(y)} j_{\delta_n}(r) + \widetilde{C}_n^{(y)} y_{\delta_n}(r) + \displaystyle\sum_{k=1}^{M} C_{k,n}^{(y)} G_k^{(\delta_n)}(r) \\ \dfrac{in G_m^{(0)}(r)}{r} = C_n^{(G_m)} j_{\delta_n}(r) + \widetilde{C}_n^{(G_m)} y_{\delta_n}(r) + \displaystyle\sum_{k=1}^{M} C_{k,n}^{(G_m)} G_k^{(\delta_n)}(r) \end{cases} \tag{85}$$

and:

$$\begin{cases} \dfrac{\partial j_0(r)}{\partial r} + \dfrac{2 j_0(r)}{r} = D_n^{(j)} j_{\delta_n}(r) + \widetilde{D}_n^{(j)} y_{\delta_n}(r) + \displaystyle\sum_{k=1}^{M} D_{k,n}^{(j)} G_k^{(\delta_n)}(r) \\ \dfrac{\partial y_0(r)}{\partial r} + \dfrac{2 y_0(r)}{r} = D_n^{(y)} j_{\delta_n}(r) + \widetilde{D}_n^{(y)} y_{\delta_n}(r) + \displaystyle\sum_{k=1}^{M} D_{k,n}^{(y)} G_k^{(\delta_n)}(r) \\ \dfrac{\partial G_m^{(0)}(r)}{\partial r} + \dfrac{2 G_m^{(0)}(r)}{r} = D_n^{(G_m)} j_{\delta_n}(r) + \widetilde{D}_n^{(G_m)} y_{\delta_n}(r) + \displaystyle\sum_{k=1}^{M} D_{k,n}^{(G_m)} G_k^{(\delta_n)}(r) \end{cases} \tag{86}$$

It should be noted that coefficients $C_n^{(j)}, \widetilde{C}_n^{(j)}, C_{k,n}^{(j)}$ etc. are stored in a library and not computed at each iteration of the minimization procedure. Hence by using together (85), (86), (74) and (13):

$$\begin{cases} F_n^{(r,p)} = \gamma_n C_n^{(j)} + \widetilde{\gamma}_n C_n^{(y)} + \displaystyle\sum_{m=1}^{M} \gamma_{m,n} C_n^{(G_m)} \\ \widetilde{F}_n^{(r,p)} = \gamma_n \widetilde{C}_n^{(j)} + \widetilde{\gamma}_n \widetilde{C}_n^{(y)} + \displaystyle\sum_{m=1}^{M} \gamma_{m,n} \widetilde{C}_n^{(G_m)} \\ F_{k,n}^{(r,p)} = \gamma_n C_{k,n}^{(j)} + \widetilde{\gamma}_n C_{k,n}^{(y)} + \displaystyle\sum_{m=1}^{M} \gamma_{m,n} C_{k,n}^{(G_m)} \end{cases} \tag{87}$$

and:

$$\begin{cases} F_n^{(\theta,p)} = \gamma_n D_n^{(j)} + \widetilde{\gamma}_n D_n^{(y)} + \displaystyle\sum_{m=1}^{M} \gamma_{m,n} D_n^{(G_m)} \\ \widetilde{F}_n^{(\theta,p)} = \gamma_n \widetilde{D}_n^{(j)} + \widetilde{\gamma}_n \widetilde{D}_n^{(y)} + \displaystyle\sum_{m=1}^{M} \gamma_{m,n} \widetilde{D}_n^{(G_m)} \\ F_{k,n}^{(\theta,p)} = \gamma_n D_{k,n}^{(j)} + \widetilde{\gamma}_n D_{k,n}^{(y)} + \displaystyle\sum_{m=1}^{M} \gamma_{m,n} D_{k,n}^{(G_m)} \end{cases} \tag{88}$$

Thus, for any $\boldsymbol{P} = (\gamma_n, \widetilde{\gamma}_n, \gamma_{1,n}, \cdots, \gamma_{M,n})_{\substack{-N\leq n\leq N \\ n\neq 0}} \in \mathcal{P}$ the following gradient holds:

$$\begin{cases} \dfrac{\partial \boldsymbol{F}_n^p}{\partial \gamma_n} = \left(C_n^{(j)}, \widetilde{C}_n^{(j)}, C_{1,n}^{(j)}, \cdots, C_{M,n}^{(j)}, D_n^{(j)}, \widetilde{D}_n^{(j)}, D_{1,n}^{(j)}, \cdots, D_{M,n}^{(j)}\right)^T \\ \dfrac{\partial \boldsymbol{F}_n^p}{\partial \widetilde{\gamma}_n} = \left(C_n^{(y)}, \widetilde{C}_n^{(y)}, C_{1,n}^{(y)}, \cdots, C_{M,n}^{(y)}, D_n^{(y)}, \widetilde{D}_n^{(y)}, D_{1,n}^{(y)}, \cdots, D_{M,n}^{(y)}\right)^T \\ \dfrac{\partial \boldsymbol{F}_n^p}{\partial \gamma_{m,n}} = \left(C_n^{(G_m)}, \widetilde{C}_n^{(G_m)}, C_{1,n}^{(G_m)}, \cdots, C_{M,n}^{(G_m)}, D_n^{(G_m)}, \widetilde{D}_n^{(G_m)}, D_{1,n}^{(G_m)}, \cdots, D_{M,n}^{(G_m)}\right)^T \end{cases} \tag{89}$$

## 7. Validation with Finite Element Model

In this section, the analytical solution derived in this paper is partially validated by comparing with a Finite Element computation performed with the free Finite Element software Castem developed by CEA (2011). It should be noted that the minimization procedure is not applied in this section (i.e., $\gamma_p = 0$) and gravity has been discarded. A semi-hollow cylinder is modeled with 160 quadrandugular elements along the radial direction and 600 along the circumferential direction. Geometrical and material parameters are listed in table 1. The following eigenstrain is imposed:

$$\begin{cases} \varepsilon_{rr}^* = \chi_{rr}^* \dfrac{(r - r_{inf})(r - r_{sup})}{r_{inf} r_{sup}} \cos(2\theta) \\ \varepsilon_{\theta\theta}^* = \chi_{\theta\theta}^* \dfrac{(r - r_{inf})(r - r_{sup})}{r_{inf} r_{sup}} \cos(2\theta) \\ \varepsilon_{r\theta}^* = \chi_{r\theta}^* \dfrac{(r - r_{inf})(r - r_{sup})}{r_{inf} r_{sup}} \cos\left(2\left(\theta + \dfrac{\pi}{4}\right)\right) \end{cases} \tag{90}$$

where $\chi_{rr}^* = \chi_{\theta\theta}^* = 0$ and $\chi_{r\theta}^* = 0.01$ (different values are tested in section 8). The imposed eigenstrain (90) is rather arbitrary, the only advantage is that induced deformations are similar to coil sagging. The vanishing condition at $r_{inf}$ and $r_{sup}$ is chosen only to facilitate the Castem computation. Indeed, the "imposed strain" option in Castem may lead to inaccuracies to verify boundary conditions. Results are presented in figure 4. A comparison between the Finite Element computation and the analytical solution is proposed in figure 5. Very good agreement is observed.

Table 1: Modeling parameters

| | | | |
|---|---|---|---|
| External radius | $r_{sup}$ | (mm) | 975 |
| Internal radius | $r_{inf}$ | (mm) | 375 |
| Lamé's coefficient | $\lambda$ | (MPa) | 98076.9 |
| Shear modulus | $\mu$ | (MPa) | 65384.6 |
| Radial stiffness coefficient | $\alpha$ | (-) | $\sqrt{1/0.3}$ |

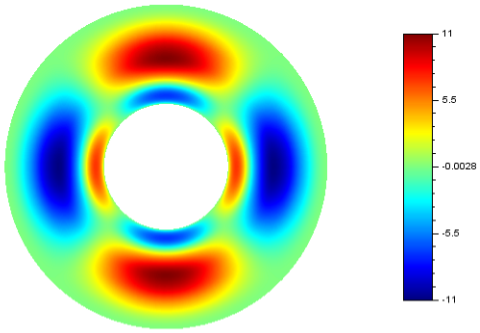


(a) $\sigma_{rr}$ (MPa)

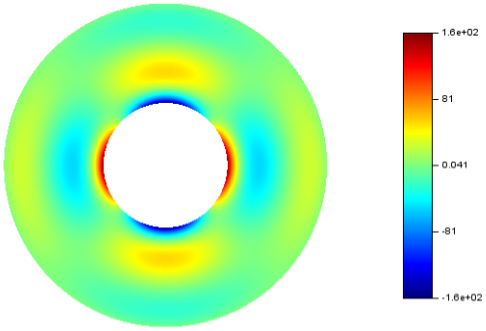


(b) $\sigma_{\theta\theta}$ (MPa)

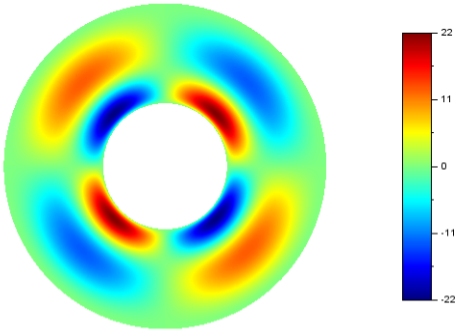


(c) $\sigma_{r\theta}$ (MPa)

Figure 4: Validation condition: stresses

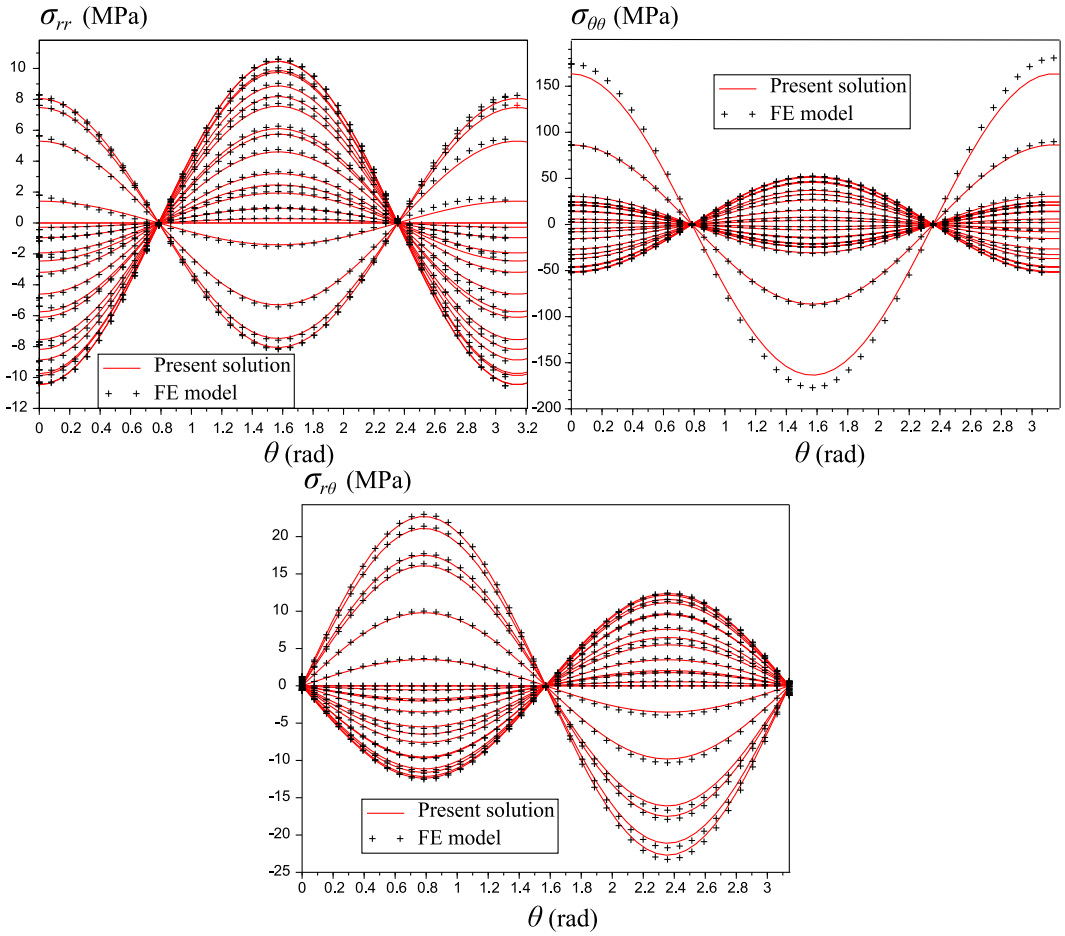


Figure 5: Validation of the analytical solution

## 8. Results

In this section, various configurations are tested in order to determine how the model behaves with respect to different parameters. In sections 8.1, 8.2, 8.3 and 8.4 the imposed eigenstrain is not realistic (variation between -0.2 to 0.2) and is only meant to force coil sagging and emphasize the influence of different parameters to give insights on coil sagging mechanisms. In particular, the role of sliding is investigated as well as non axi-symmetric loading conditions, shear threshold and radial stiffness. Material parameters are listed in table 1 and the eigenstrain is given in the form of (90). This analytical form is rather arbitrary even though the quadratic evolution along the radial direction schematically corresponds to the eigenstrain analyzed in Weisz-Patrault (2017a, 2018). All tested conditions are listed in table 2. All following figures are given on the deformed configuration without amplification factor applied on displacements. However, some figures are scaled down so that all figures have the same size.

The effect of gravity is investigated in section 8.5 in order to determine to what extent it can explain the coil sagging phenomenon. Finally, on the basis of the proposed mechanisms and on the previous contribution published by Weisz-Patrault (2018), realistic conditions promoting coil sagging are discussed in section 8.6.

Table 2: Loading conditions

| Condition | $\chi^*_{rr}$ | $\chi^*_{\theta\theta}$ | $\chi^*_{r\theta}$ |
|---|---|---|---|
| 1 | 0.8 | 0 | 0 |
| 2 | 0 | -0.8 | 0 |
| 3 | 0 | 0 | -0.8 |

### *8.1. Effect of the dimension of the minimization space*

The critical stress $\sigma_C$ (defined by (81)) is interpreted as a threshold for the shear stress $\sigma_{r\theta}$. For condition 2, $\sigma_C$ is set to 0, thus the minimization process should lead to $\sigma_{r\theta} = 0$. However, the minimization is done on the parameter space $\mathcal{P}_2$ that is only a finite dimensional subspace of the infinite dimensional space of continuous functions. As a result, the shear stress does not vanish because the minimum is not reached. However, the shear stress and the total energy $E - W + D$ decrease as the dimension of $\mathcal{P}_2$ increases, as shown in figures 6 and 7. It should be noted that even though convergence is not strictly reached for $M = 15$ because the shear stress level still does not vanish, the overall shape (displacement) does not evolve much from $M = 10$ to $M = 15$. Maximum shear stresses seem to converge toward zero as expected (29,6.6,2.8 MPa for $M = 5, 10$ and 15 respectively). Thus, even though the convergence is not strictly reached, it is not relevant to increase too much $M$ because the prediction of sagging is already captured with $M = 15$, of course larger values of $M$ would give more accurate stresses, but without major improvements on the final shape of the coil.

Oscillations along the radial direction clearly affect stresses. These oscillations are related to $M$. Maxima are overestimated, but increasing $M$ leads to increase the oscillation frequency and to reduce the oscillation amplitude. Nevertheless it is very likely that $M$ cannot be increased indefinitely as numerical errors due to matrix inversions would be significantly amplified as noticed for instance by Weisz-Patrault et al. (2011, 2013) for ill-posed problems. This issue is a common limitation to most series expansions. In this contribution, $M = 15$ has been found as a good compromise.

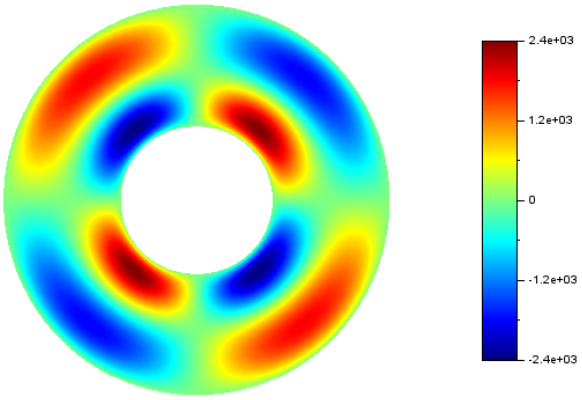


(a) $\sigma_{r\theta}$ (MPa) ($\gamma^p = 0$)

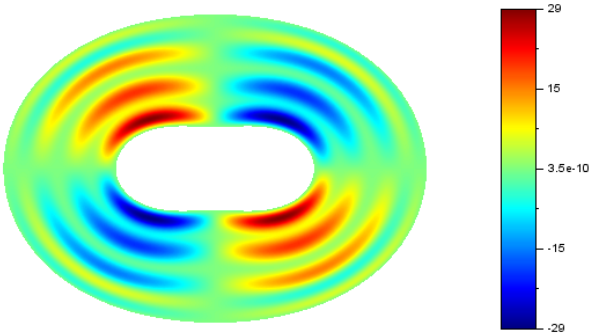


(b) $\sigma_{r\theta}$ (MPa) ($M = 5$)

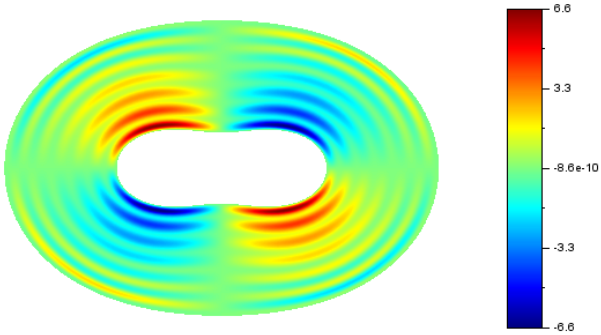


(c) $\sigma_{r\theta}$ (MPa) ($M = 10$)

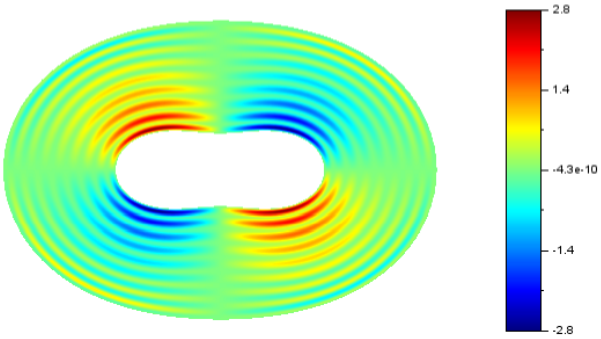


(d) $\sigma_{r\theta}$ (MPa) ($M = 15$)

Figure 6: Condition 2: Convergence of the minimization procedure ($\sigma_C = 0$)

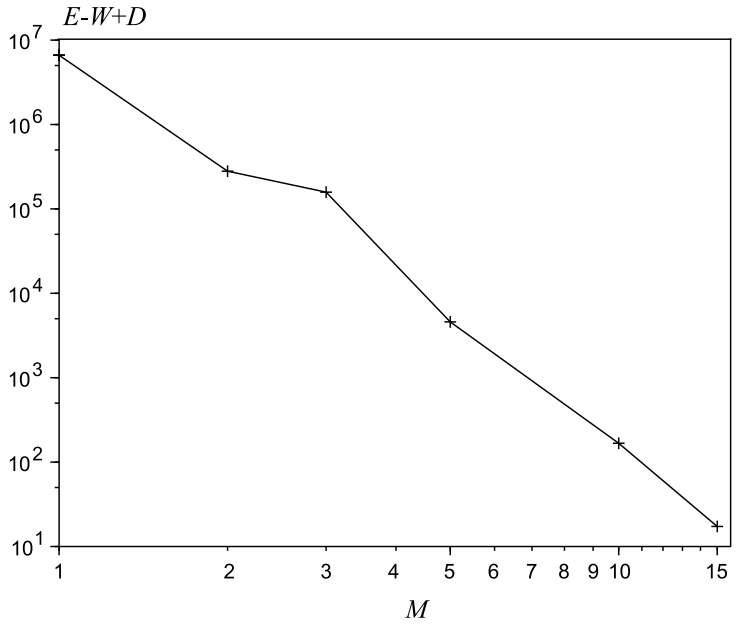


Figure 7: Condition 2: Convergence of the minimization procedure ($\sigma_C = 0$)

*8.2. Effect of the eigenstrain*

Conditions listed in table 2 are presented in figures 8, 9 and 10. Conditions 1 and 2 lead to coil sagging. It should be noted that effect of $\varepsilon^*_{rr}$ is opposite to $\varepsilon^*_{\theta\theta}$ with respect to the sagging direction (one condition tends to deform the coil as sagging does and the other one has the same effect but rotated by 90 degrees). However, the analysis proposed by Weisz-Patrault (2018) shows that the radial and circumferential components are almost similar which in turn reduces the coil sagging effect. In addition, the imposed eigenstrain is not realistic because it is necessary to set the eigenstrain to extremely large values in order to obtain coil sagging.

The imposed shear component in condition 3 cannot significantly contribute to coil sagging. Indeed, if there is no dissipation the whole shear component of the imposed eigenstrain is compensated by the plastic-like shear strain and there is no deformation, as shown in figure 10. Reciprocally, if the shear threshold goes to infinity there is no plastic-like shear strain and the imposed shear component of the eigenstrain generates coil sagging. However, this condition is unlikely because it necessitates both very large shear threshold and eigenstrain.

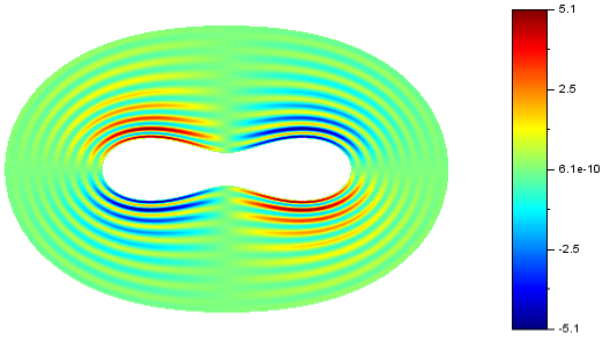


(a) $\sigma_{r\theta}$ (MPa)

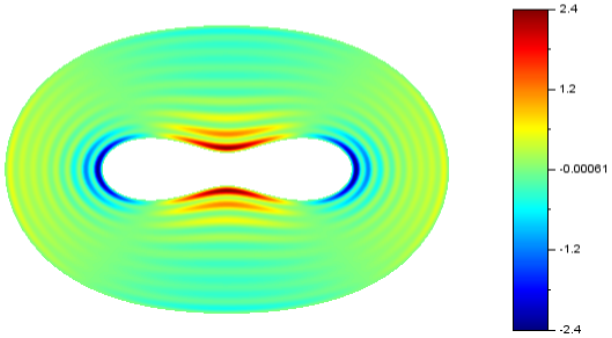


(b) $\sigma_{rr}$ (MPa)

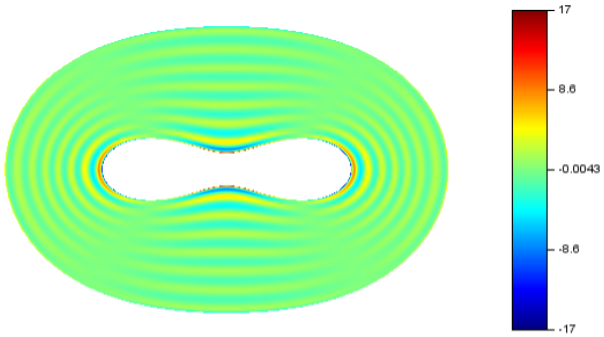


(c) $\sigma_{\theta\theta}$ (MPa)

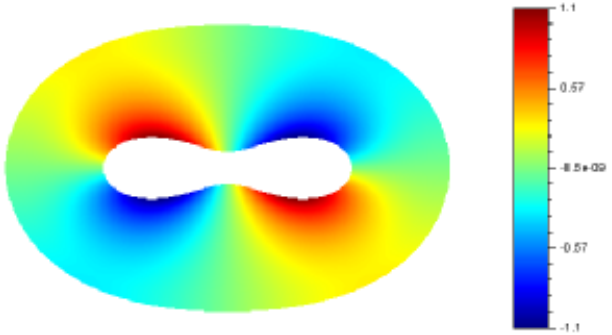


(d) $\gamma^p$

Figure 8: Condition 1 ($\sigma_C = 0, \chi^*_{rr} \neq 0$)

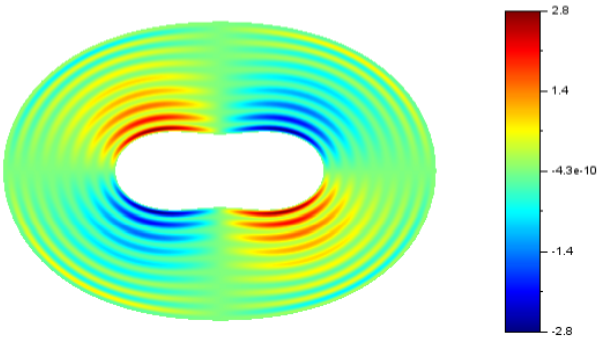


(a) $\sigma_{r\theta}$ (MPa)

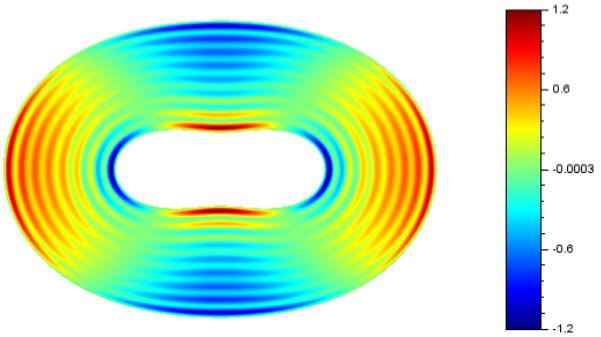


(b) $\sigma_{rr}$ (MPa)

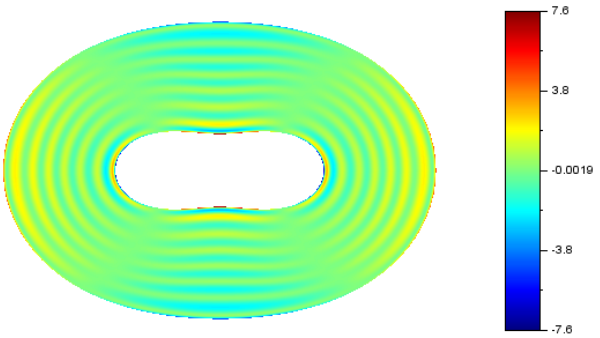


(c) $\sigma_{\theta\theta}$ (MPa)

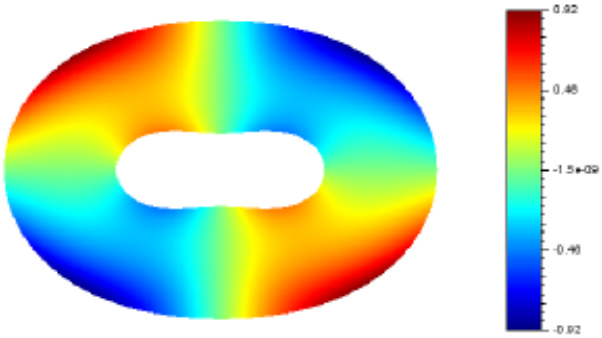

(d) $\gamma^p$

Figure 9: Condition 2 ($\sigma_C = 0, \chi^*_{\theta\theta} \neq 0$)

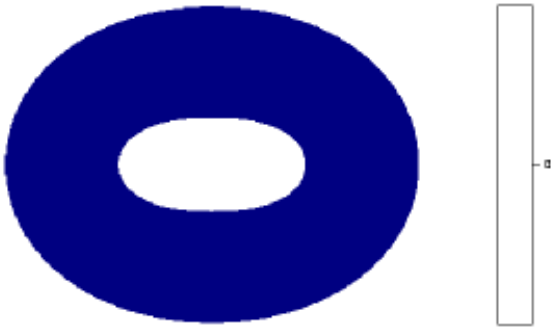

(a) $\gamma^p$ for $\sigma_C = +\infty$

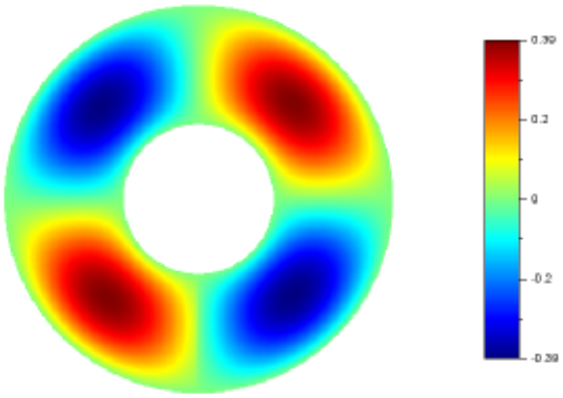

(b) $\gamma^p$ for $\sigma_C = 0$

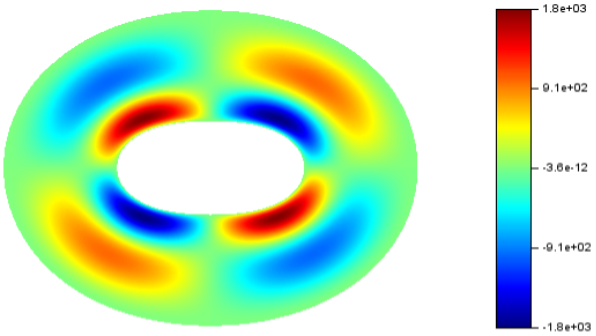


(c) $\sigma_{r\theta}$ (MPa) for $\sigma_C = +\infty$

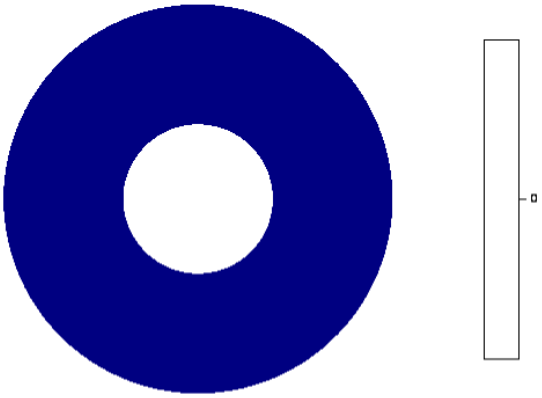

(d) $\sigma_{r\theta}$ (MPa) for $\sigma_C = 0$

Figure 10: Condition 3 ($\chi^*_{r\theta} \neq 0$)

### *8.3. Effect of dissipation*

It is clear that large sliding (represented by the plastic-like shear strain $\gamma^p$) is a necessary condition for coil sagging to occur. Thus, the dissipation cost (associated to $\gamma^p$) control the intensity of coil sagging effects. The shear threshold $\sigma_C$ is set at different values. Resulting $\gamma^p$ are presented in figure 11. The plastic-like shear strain amplitude and displacements rapidly decrease as the shear threshold increases. The simple relationship (81) is used to determine what are realistic values of $\sigma_C$. The friction coefficient is set to $f_C \approx 0.1$ (realistic for lubricated contacts) and previous computations performed by Weisz-Patrault (2018) under axi-symmetric assumption found contact pressures approximately between 0.1 MPa and 20 MPa (depending on the progress of coil cooling), which leads approximately to $0.02 \leq \sigma_C \leq 3.5$. Thus, $\sigma_C \leq 0.02$ is not realistic. It should be noted that coil sagging is negligible for $\sigma_C = 0.1$ MPa even though the imposed eigenstrain is very intense. This indicates that non axi-symmetric eigenstrains are not directly responsible for the coil sagging phenomenon.

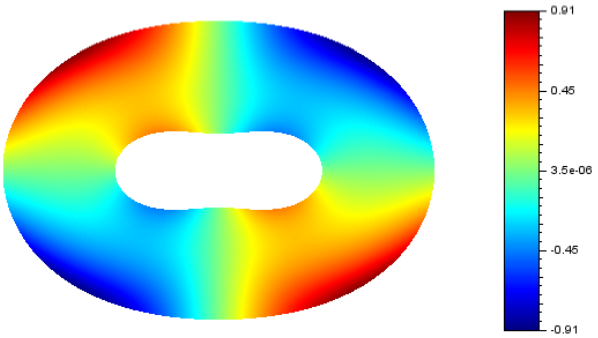


(a) $\sigma_C = 0.0001$ (MPa)

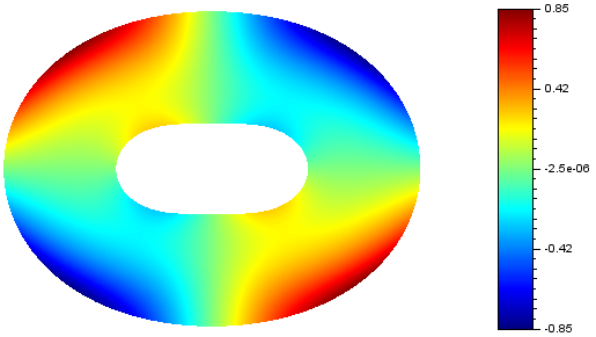


(b) $\sigma_C = 0.001$ (MPa)

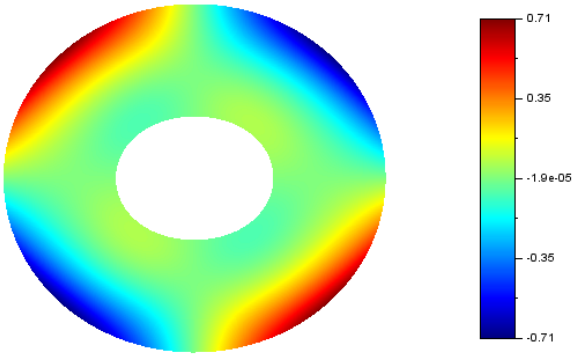


(c) $\sigma_C = 0.01$ (MPa)

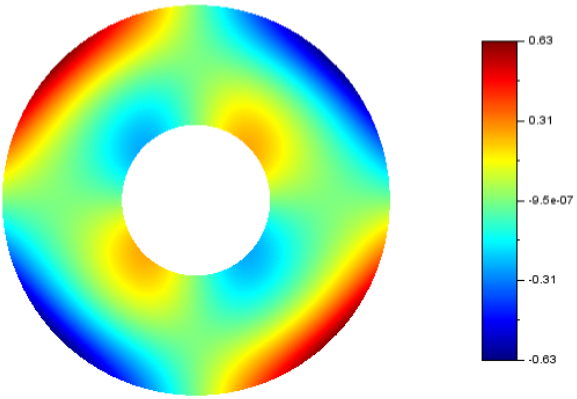


(d) $\sigma_C = 0.1$ (MPa)

Figure 11: Condition 2: $\gamma^p$ ($M = 15$), effect of dissipation

### *8.4. Effect of radial stiffness*

The radial stiffness depends on the contact roughness and the number of interfaces (i.e., for a fixed upper and lower radii $r_{inf}$ and $r_{sup}$ the number of interface is determined by layer thicknesses). The effect of radial stiffness is demonstrated in figure 12. Deformations increase as the radial stiffness increases. This result may appear counter-intuitive. However, when the radial stiffness increases, the elastic energy would increase if plastic-like shear strain were identical. Since $\sigma_C = 0$ (i.e., sliding does not cost energy) it is more energetically profitable to increase $\gamma^p$ (and therefore the coil sagging effect) in order to decrease the elastic bulk energy. Thus, roughness is a key parameter that prevent coil sagging because the shear threshold is higher for rough surface and the radial stiffness is lower.

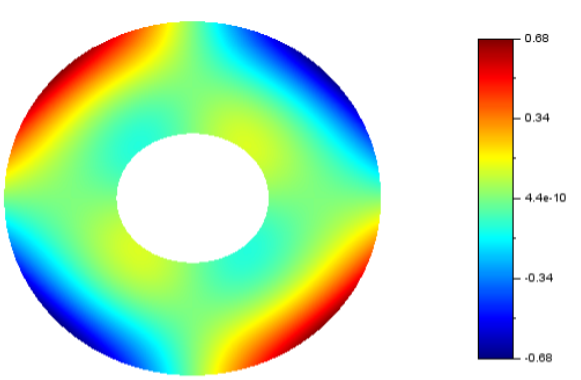


(a) $1/\alpha^2 = 0.25$

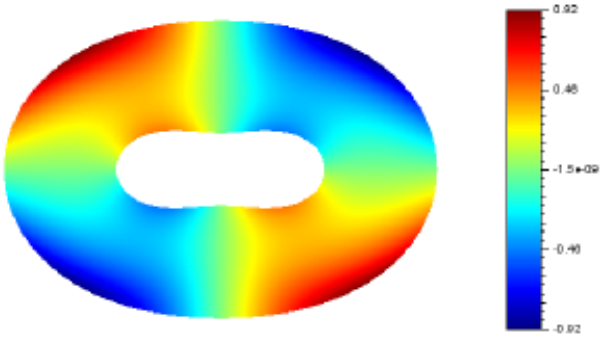

(b) $1/\alpha^2 = 0.3$

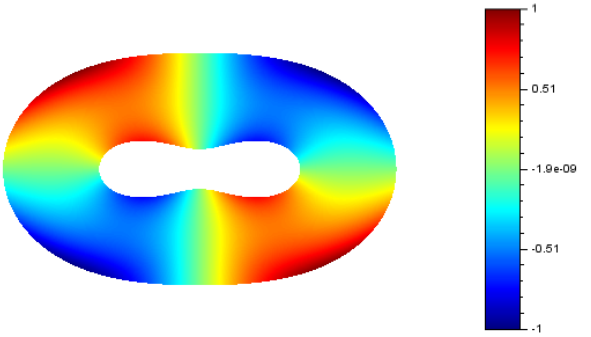


(c) $1/\alpha^2 = 0.35$

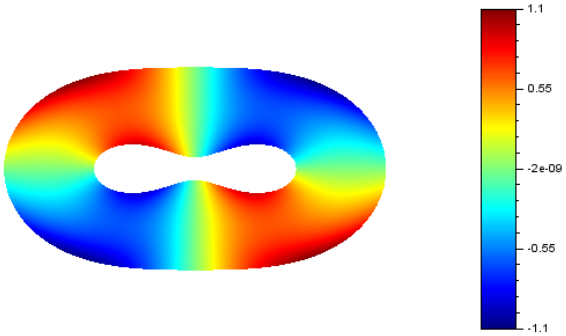


(d) $1/\alpha^2 = 0.4$

Figure 12: Condition 2: $\gamma^p$ ($M = 15$), effect of radial stiffness

### *8.5. Effect of gravity*

Conditions including gravity are much more difficult to compute than conditions with eigenstrain only. This is due to the fact that the imposed eigenstrain has been chosen proportional to specific Fourier harmonics $(\cos(n\theta), \sin(n\theta))$ (where $n = 2$ in this paper). Thus it is sufficient to minimize on the subspace $\mathcal{P}_n$ with a fixed $n$. However, even though the body force $\rho g$ introduced by gravity is proportional to the first Fourier harmonic $(\cos(\theta), \sin(\theta))$ the traction $\boldsymbol{T}$ due to the support reaction is a distribution that spreads on all Fourier harmonics $(\cos(n\theta), \sin(n\theta))$ where $n \in \mathbb{N}$. When gravity is accounted for, the work of external forces $W$ significantly contribute to the minimization procedure and the subspace $\mathcal{P}$ defined by (76) should be considered for a range $-N \leq n \leq N$. In order to avoid additional computation time, $N$ is set to 2 in following examples. As a result, the support reaction does not localize on a single point (for $\theta_0 = 0$) but spreads on a much larger area. However, since the resultant force is exactly the same, the general structural effect of weight is well captured.

The work of external forces is due to the body force $\rho g$ and to the traction applied by the support. Thus, since gravity is constant, the work of external forces depends only on the magnitude of displacements. The main deformation mechanism is that sliding represented by $\gamma^p$ enables the system to deform significantly by storing elastic energy which is widely compensated by the work of external forces (increasing with displacements). Indeed, the external work

grows much faster than the stored energy as the hollow cylinder deforms. Thus, the dissipation associated to the plastic-like shear strain is the main counterpart to this mechanism. For instance, coil sagging is obtained for $1/\alpha^2 = 0.3$ and a shear threshold $\sigma_C = 0.1$ MPa (which is a realistic value according to the idea developed in section 8.3) as shown in figure 13. This result should be compared to figure 11d that shows that no significant coil sagging is obtained under the same conditions by applying only the eigenstrain even though the amplitude of the latter is extremely large. Thus, the main mechanism leading to coil sagging is more likely due to gravity than to a non axi-symmetric eigenstrain.

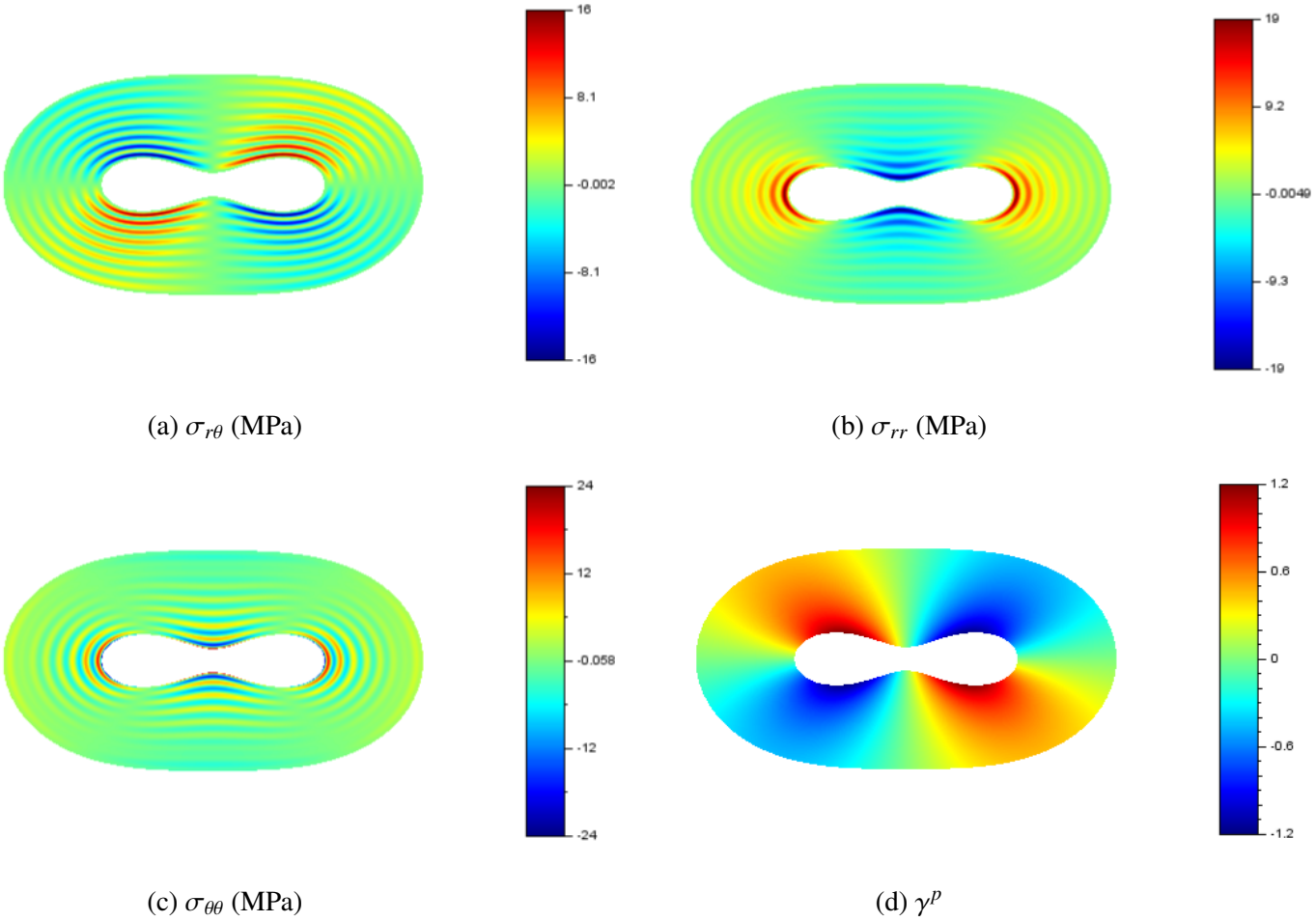


(a) $\sigma_{r\theta}$ (MPa)

(b) $\sigma_{rr}$ (MPa)

(c) $\sigma_{\theta\theta}$ (MPa)

(d) $\gamma^p$

Figure 13: Condition with gravity only: $\sigma_C = 0.1$

### *8.6. Conditions promoting coil sagging*

Different loading conditions (leading to coil sagging) have been presented and analyzed. However, extremely high eigenstrain levels that are not realistic are necessary to observe coil sagging although gravity alone may explain this phenomenon. In addition, low values of shear threshold significantly promote the phenomenon that is to say that relatively low contact pressure are necessary. The analysis proposed by Weisz-Patrault (2018) suggests that the eigenstrain (representing thermal expansion, phase transition and transformation induced plasticity) tends to decrease contact pressures during the cooling of the coil. Thus, the eigenstrain under-

lies the coil sagging phenomenon because it creates the necessary conditions more than it is the direct causal mechanism that should be attributed to gravity.

However, further investigations are necessary to determine if large non axi-symmetric eigenstrain may occur because of the non-linear nature of transformation induced plasticity. Indeed, the axi-symmetric model proposed by Weisz-Patrault (2018) consists in computing at each time step the eigenstrain increment as a function of the total stress of the previous time step. It is therefore possible that the additional stress introduced by considering gravity, generate a non axi-symmetric eigenstrain that tends to amplify. This hypothesis may be verified by coupling the model proposed in this contribution and the numerical simulation proposed by Weisz-Patrault (2018).

## 9. Conclusion

A mixed analytic/energetic approach has been proposed for a multilayer hollow cylinder accounting for sliding at the interfaces. The homogenized problem is orthotropic because of contact roughness that tends to decrease the radial stiffness. Sliding is homogenized by the introduction of a plastic-like shear strain that is determined by an energetic principle and a minimization procedure based on a quasi-Newton algorithm. The hollow cylinder is subjected to gravity and a non axi-symmetric eigenstrain representing phase transitions.

This problem is applied to the numerical simulation of coil sagging. Deformation mechanisms have been investigated and results suggest that gravity associated to low shear threshold are responsible for the coil sagging phenomenon instead of non axi-symmetric eigenstrain. Thus, the major role played by the eigenstrain is to promote favorable conditions. Indeed, previous studies show that thermal expansion, phase transition and transformation induced plasticity tends to decrease contact pressures and therefore the shear threshold.

## Appendix A. Boundary condition

The resultant weight (per unit width) is:

$$\boldsymbol{F}_W = -\pi\left(r_{sup}^2 - r_{inf}^2\right)\rho g \boldsymbol{e}_y \tag{A.1}$$

The resultant force of surface traction (per unit width) is:

$$F_S\left(\boldsymbol{e}_r(\theta_0) + \boldsymbol{e}_r(\pi-\theta_0)\right) = 2F_S\sin(\theta_0)\boldsymbol{e}_y \tag{A.2}$$

The equilibrium gives:

$$F_S = -\frac{\pi\left(r_{sup}^2 - r_{inf}^2\right)\rho g}{2\sin(\theta_0)} \tag{A.3}$$

Furthermore if $T_r^{sup}(\theta) = f_S\left(\delta_{\theta_0}(\theta) + \delta_{\pi-\theta_0}(\theta)\right)$:

$$F_S\left(\boldsymbol{e}_r(\theta_0) + \boldsymbol{e}_r(\pi-\theta_0)\right) = \int_0^{2\pi} T_r^{sup}(\theta)\boldsymbol{e}_r(\theta)r_{sup}\mathrm{d}\theta = f_S\, r_{sup}\left(\boldsymbol{e}_r(\theta_0) + \boldsymbol{e}_r(\pi-\theta_0)\right) \tag{A.4}$$

Hence:

$$T_r^{sup}(\theta) = -\frac{\pi\left(r_{sup}^2 - r_{inf}^2\right)\rho g}{2\sin(\theta_0)r_{sup}}\left(\delta_{\theta_0}(\theta) + \delta_{\pi-\theta_0}(\theta)\right) \tag{A.5}$$

## Appendix B. Critical shear stress

The critical shear stress $\sigma_C$ arises in the dissipation (79) for the homogenized model (see figure 2). Thus, $\sigma_C$ is defined so that the dissipated energy in the homogenized model is equal to the dissipated energy due to sliding in the non-homogenized model.The non-homogenized model is composed of a large number of interfaces. Let $r^i$ denote the radius of the $i$-th interface, $\Delta u^i_\theta(\theta)$ denote the tangential displacement jump (sliding) and $\sigma^i_{rr}(\theta)$ and $\sigma^i_{r\theta}(\theta)$ denote the contact pressure and shear stress at the $i$-th interface. A classic Coulomb friction law is assumed:

$$\sigma^i_{r\theta} = f_C \sigma^i_{rr} \tag{B.1}$$

where the friction coefficient $f_C$ is assumed to be constant, which is a reasonable assumption considering the studied process (homogenous roughness and controlled lubrication conditions). Therefore, if sliding is the only dissipative mechanism, the dissipated energy per unit width of an infinitesimal length of the $i$-th interface reads:

$$\delta D^i = \left|\Delta u^i_\theta(\theta)\right| f_C \sigma^i_{rr}(\theta) r^i \mathrm{d}\theta \tag{B.2}$$

For the homogenized model, the plastic shear $\gamma^p$ controls the only dissipative mechanism and the corresponding dissipated energy per unit width of an infinitesimal volume is:

$$\delta D = \sigma_C \gamma^p_{cum}(r,\theta) r \mathrm{d}r \mathrm{d}\theta \tag{B.3}$$

In the homogenized continuous model, d$r$ represents $I$ interfaces, that is to say that if $t$ denotes the layer thickness $\mathrm{d}r = I \times t$. Thus the dissipated energy per unit width in the homogenized model is the sum of the dissipated energies per unit width by the $I$ corresponding interfaces (denoted by $\{i_1, \cdots, i_I\}$):

$$\delta D = \sum_{i=i_1}^{i_I} \delta D^i \tag{B.4}$$

Hence:

$$\sigma_C \gamma^p_{cum}(r,\theta) r \mathrm{d}r \mathrm{d}\theta = \sum_{i=i_1}^{i_I} \left|\Delta u^i_\theta(\theta)\right| f_C \sigma^i_{rr}(\theta) r^i \mathrm{d}\theta \tag{B.5}$$

For the sake of simplicity, it is assumed that:

$$\begin{cases} r^i \approx r \\ \Delta u^i_\theta(\theta) \approx \dfrac{1}{I} \displaystyle\sum_{i=i_1}^{i_I} \Delta u^i_\theta(\theta) = \Delta u_\theta(r,\theta) \\ \sigma^i_{rr}(\theta) \approx \dfrac{1}{I} \displaystyle\sum_{i=i_1}^{i_I} \sigma^i_{rr} = P_C(r,\theta) \end{cases} \tag{B.6}$$

where $P_C$ is defined as the averaged contact pressure. These assumptions are reasonable as the problem consists in thin layers (variations of $r^i$, $\Delta u^i_\theta$ and $\sigma^i_{rr}$ for $i_1 \leq i \leq i_I$ are small). Hence:

$$\sigma_C(r,\theta)\gamma^p_{cum}(r,\theta) = f_C P_C(r,\theta) \frac{|\Delta u_\theta(r,\theta)|}{t} \tag{B.7}$$

By neglecting the effect of elastic strains on the homogenization procedure, the strain $\gamma^p$ can be defined as:

$$\gamma^p(r,\theta) = \frac{\Delta u_\theta(r,\theta)}{t} \tag{B.8}$$

Thus from (B.7) and (80):

$$\sigma_C(r,\theta) = \sqrt{3} f_C P_C(r,\theta) \tag{B.9}$$

For the sake of simplicity, $\sigma_C$ has been taken constant in the minimization procedure (82), which is a reasonable approximation considering numerical results provided by Weisz-Patrault (2018).

## References


Abd-Alla, A., Mahmoud, S., 2010. Magneto-thermoelastic problem in rotating non-homogeneous orthotropic hollow cylinder under the hyperbolic heat conduction model. Meccanica 45, 451–462.

Bluthé, J., Weisz-Patrault, D., Ehrlacher, A., 2017. Energetic approach for a sliding inclusion accounting for plastic dissipation at the interface, application to phase nucleation. International Journal of Solids and Structures 121, 163–173.

Bree, J., 1989. Plastic deformation of a closed tube due to interaction of pressure stresses and cyclic thermal stresses. International journal of mechanical sciences 31, 865–892.

CEA, 2011. Cast3m. Commissariat A l'Energie Atomique, http://www-cast3m.cea.fr/.

Chatzigeorgiou, G., Charalambakis, N., Murat, F., 2009. Homogenization of a pressurized tube made of elastoplastic materials with discontinuous properties. International Journal of Solids and Structures 46, 3902–3913.

Edwards, W., Boulton, G., 2001. The mystery of coil winding, in: 2001 Iron and Steel Exposition and AISE Annual Convention, pp. 2001–2017.

El-Naggar, A., Abd-Alla, A., Fahmy, M., Ahmed, S., 2002. Thermal stresses in a rotating non-homogeneous orthotropic hollow cylinder. Heat and Mass Transfer 39, 41–46.

Eraslan, A.N., Akis, T., 2006. Plane strain analytical solutions for a functionally graded elastic–plastic pressurized tube. International Journal of Pressure Vessels and Piping 83, 635–644.

Fedelich, B., Ehrlacher, A., 1997. An analysis of stability of equilibrium and of quasi-static transformations on the basis of the dissipation function. European journal of mechanics. A. Solids 16, 833–855.

Hou, P.F., Leung, A.Y., 2004. The transient responses of magneto-electro-elastic hollow cylinders. Smart Materials and Structures 13, 762.

Hudzia, J., Ferrauto, F., Gevers, P., 1994. Stress calculation applied to a coil, and optimization of coiling tension. Cah. Inf. Tech. Rev. Metall. 91, 937–943.

Kalam, M., Tauchert, T., 1978. Stresses in an orthotropic elastic cylinder due to a plane temperature distribution t (r, $\theta$). Journal of thermal stresses 1, 13–24.

Kardomateas, G., 1990. The initial phase of transient thermal stresses due to general boundary thermal loads in orthotropic hollow cylinders. Journal of applied mechanics 57, 719–724.

Kedl, D., 1992. using a two dimensional winding model to predict wound roll stresses that occur due to circumferential steps in core diameter or to cross-web caliper variation, in: Proceedings of the Second International Conference on Web Handling, pp. 99–112.

Lekhnitskii, S., Fern, P., Brandstatter, J.J., Dill, E., 1964. Theory of elasticity of an anisotropic elastic body. Physics Today 17, 84.

Mielke, A., 2003. Energetic formulation of multiplicative elasto-plasticity using dissipation distances. Continuum Mechanics and Thermodynamics 15, 351–382.

Muskhelishvili, N., 1953. Some basic problems of the mathematical theory of elasticity. Noordhoff International Publishing, Groningen. 2nd edition (1977).

Ou, Z.C., Chen, Y.H., 2007. General solution of the stress potential function in lekhnitskii's elastic theory for anisotropic and piezoelectric materials. Adv Stud Theor Phys 1, 357–366.

Pagano, N.J., 1994. The stress field in a cylindrically anisotropic body under two-dimensional surface tractions, in: Mechanics of Composite Materials. Springer, pp. 151–156.

Pronina, Y., 2013. Analytical solution for the general mechanochemical corrosion of an ideal elastic–plastic thick-walled tube under pressure. International Journal of Solids and Structures 50, 3626–3633.

Wadsley, A., Edwards, W., 1977. Coil winding stresses. J. Australas. Inst. Met. 22, 17–27.

Weisz-Patrault, D., 2017a. Coupled heat conduction and multiphase change problem accounting for thermal contact resistance. International Journal of Heat and Mass Transfer 104, 595–606.

Weisz-Patrault, D., 2017b. Multiphase model for transformation induced plasticity. extended leblond's model. Journal of the Mechanics and Physics of Solids 106, 152–175.

Weisz-Patrault, D., 2018. Nonlinear and multiphysics evaluation of residual stresses in coils. Applied Mathematical Modelling 61, 141–166.

Weisz-Patrault, D., Bock, S., Gürlebeck, K., 2014. Three-dimensional elasticity based on quaternion-valued potentials. International Journal of Solids and Structures 51, 3422–3430.

Weisz-Patrault, D., Ehrlacher, A., 2017. Imposed curvature of an elastic-plastic strip: application to simulation of coils. Mechanics & Industry 18, 218–228.

Weisz-Patrault, D., Ehrlacher, A., Legrand, N., 2011. A new sensor for the evaluation of contact stress by inverse analysis during steel strip rolling. Journal of Materials Processing Technology 211, 1500–1509.

Weisz-Patrault, D., Ehrlacher, A., Legrand, N., 2013. Evaluation of contact stress during rolling process, by three dimensional analytical inverse method. International Journal of Solids and Structures 50, 3319 – 3331.

Weisz-Patrault, D., Ehrlacher, A., Legrand, N., 2016. Non-linear simulation of coiling accounting for roughness of contacts and multiplicative elastic-plastic behavior. International Journal of Solids and Structures 94-95, 1–20.

Weisz-Patrault, D., Ehrlacher, A., Legrand, N., Mathey, E., 2015. Non-linear numerical simulation of coiling by elastic finite strain model. Key Engineering Materials 651-653, 1060–1065.

Ye, J., Soldatos, K., 1994. Three-dimensional stress analysis of orthotropic and cross-ply laminated hollow cylinders and cylindrical panels. Computer Methods in Applied Mechanics and Engineering 117, 331–351.

Yee, K.C., Moon, T., 2002. Plane thermal stress analysis of an orthotropic cylinder subjected to an arbitrary, transient, asymmetric temperature distribution. Journal of applied mechanics 69, 632–640.